NASA TECHNICAL MEMORANDUM

NASA TM X-2611

NASA TM X-2611

EFFECT OF CONFIGURATION MODIFICATIONS ON THE HYPERSONIC AERODYNAMIC CHARACTERISTICS OF A BLENDED DELTA WING-BODY ENTRY VEHICLE

by James P. Arrington and George C. Ashby, Jr.

Langley Research Center

Hampton, Va. 23365

NATIONAL AERONAUTICS AND SPACE ADMINISTRATION • WASHINGTON, D. C. • SEPTEMBER 1972

1. Report No.	2. Government Accession No.	3. Recipient's Catalog No.
NASA TM X-2611		

4. Title and Subtitle	5. Report Date
EFFECT OF CONFIGURATION MODIFICATIONS ON THE HYPERSONIC AERODYNAMIC CHARACTERISTICS OF A BLENDED DELTA WING-BODY ENTRY VEHICLE	September 1972
	6. Performing Organization Code

7. Author(s)	8. Performing Organization Report No.
James P. Arrington and George C. Ashby, Jr.	L-8419
	10. Work Unit No. 502-37-01-04
9. Performing Organization Name and Address NASA Langley Research Center Hampton, Va. 23365	11. Contract or Grant No.
	13. Type of Report and Period Covered Technical Memorandum
2. Sponsoring Agency Name and Address National Aeronautics and Space Administration Washington, D.C. 20546	14. Sponsoring Agency Code

5. Supplementary Notes

6. Abstract

This study includes the longitudinal, lateral, and directional aerodynamic characteristics of a delta-wing configuration obtained experimentally at Mach 20 in helium with Reynolds numbers, based on model length, of 1.5×10^6 and 2.9×10^6 and at a Mach number of 6 in air with a Reynolds number, based on model length, of 4.8×10^6. The angles of attack varied from 0^o to 55^o for two sideslip angles. The effects of the addition of dorsal fins, the removal of wing tip fins, an increase in elevon span, and changes in elevon hinge-line sweep angle are discussed. The unmodified vehicle had a maximum lift-drag ratio of 2.1 at Mach 19 and of 2.4 at Mach 6 with about the same lateral and directional stability level at both Mach numbers. As the Mach number increased from 6 to 20, the longitudinal center of pressure moved forward and a more positive elevon deflection was therefore required to maintain a given trim angle. The removal of wing tip fins increased the maximum lift-drag ratio and had a negligible effect on longitudinal stability, but caused directional instability that was not corrected by the dorsal fins examined. The shape of the wing and elevon hinge-line sweep had a large influence on the induced yawing moment due to roll control.

7. Key Words (Suggested by Author(s))	18. Distribution Statement
Space shuttle orbiter Blended delta wing-body Hypersonic aerodynamic characteristics	Unclassified - Unlimited

19. Security Classif. (of this report)	20. Security Classif. (of this page)	21. No. of Pages	22. Price*
Unclassified	Unclassified	57	$3.00

.EFFECT OF CONFIGURATION MODIFICATIONS ON THE HYPERSONIC AERODYNAMIC CHARACTERISTICS OF A BLENDED DELTA WING-BODY ENTRY VEHICLE

By James P. Arrington and George C. Ashby, Jr.
Langley Research Center

SUMMARY

A part of a continuing evaluation of space shuttle concepts and their evolutionary changes are presented. The study included the longitudinal, lateral, and directional aerodynamic characteristics of a blended delta wing-body entry configuration obtained experimentally at Mach numbers near 20 in helium with Reynolds numbers, based on model length, of 1.5×10^6 and 2.9×10^6 and at a Mach number of 6 in air with a Reynolds number, based on model length, of 4.8×10^6. The angles of attack varied from 0^o to 55^o for two sideslip angles.

The investigation included the effects of the addition of dorsal fins, the removal of wing tip fins, an increase in elevon span, and changes in elevon hinge-line sweep angle. The unmodified vehicle had a maximum lift-drag ratio of 2.1 at Mach 19 and of 2.4 at Mach 6 with about the same lateral and directional stability level at both Mach numbers. As the Mach number increased, the longitudinal center of pressure moved forward and a more positive elevon deflection was therefore required to maintain a given trim angle. The removal of wing tip fins from the vehicle increased the maximum lift-drag ratio and had a negligible effect on longitudinal stability, but caused directional instability that was not corrected by the dorsal fins examined. The shape of the wing and the elevon hinge-line sweep had a large influence on the induced yawing moment due to roll control.

INTRODUCTION

The space shuttle system is being designed to reduce the cost of transporting men and equipment to and from near-earth orbit by capitalizing on reusability (refs. 1 to 5). As the program progressed through the feasibility stage (Phase A) into the preliminary design stage (Phase B), several candidate orbiter concepts were proposed (refs. 6 to 9). The delta-wing concept has been among these candidates from the beginning.

In the ongoing process of evaluating design concepts and their evolutionary changes resulting from aerothermodynamic and structural weight analyses, one of the early delta-wing designs was continuously altered and the effects of a part of these changes on the

aerodynamic characteristics have been investigated. Although this study was conducted on an early shuttle vehicle, the results contained in this paper should be applicable to delta-wing concepts in general. This paper presents the static longitudinal, lateral, and directional aerodynamic characteristics of this delta-wing configuration for angles of attack from 0^{o} to 55^{o} at Mach 20 in helium with Reynolds numbers, based on model length, of 1.5×10^{6} and 2.9×10^{6} and at Mach 6 in air with a Reynolds number, based on model length, of 4.8×10^{6}.

SYMBOLS

The longitudinal data are referenced to both the body (C_N, C_A, and C_m) and stability (C_L and C_D) systems of axes. The lateral and directional data are referred to the body system of axes only. The location of the moment reference center is shown in figure 1.

C_A axial-force coefficient, $\frac{\text{Axial force}}{qS}$

C_D drag coefficient, $C_A \cos \alpha + C_N \sin \alpha$

C_L lift coefficient, $C_N \cos \alpha - C_A \sin \alpha$

$C_{L,max}$ maximum lift coefficient

C_l rolling-moment coefficient, $\frac{\text{Rolling moment}}{qSl}$

C_{l_β} rate of change of rolling-moment coefficient with sideslip angle, $\Delta C_l / \Delta \beta$, per deg

$C_{l_{\delta_a}}$ rate of change of rolling-moment coefficient with aileron deflection angle, $\Delta C_l / \Delta \delta_a$, per deg

C_m pitching-moment coefficient, $\frac{\text{Pitching moment}}{qSl}$

C_N normal-force coefficient, $\frac{\text{Normal force}}{qS}$

C_n yawing-moment coefficient, $\frac{\text{Yawing moment}}{qSl}$

C_{n_β} rate of change of yawing-moment coefficient with sideslip angle, $\Delta C_n / \Delta \beta$, per deg

$C_{n_{\delta_a}}$ rate of change of yawing-moment coefficient with aileron deflection angle, $\Delta C_n/\Delta\delta_a$, per deg

C_Y side-force coefficient, $\frac{\text{Side force}}{qS}$

C_{Y_β} rate of change of side-force coefficient with sideslip angle, $\Delta C_Y/\Delta\beta$, per deg

$C_{Y_{\delta_a}}$ rate of change of side-force coefficient with aileron deflection angle, $\Delta C_Y/\Delta\delta_a$, per deg

L/D lift-drag ratio, C_L/C_D

l body length

M Mach number

q dynamic pressure

R Reynolds number, based on body length

r radius

S reference planform area

x longitudinal coordinate, measured from model nose

Y lateral coordinate, measured from model center line

α angle of attack, deg

β sideslip angle, deg

δ_a aileron deflection angle, $\frac{\delta_{e,left} - \delta_{e,right}}{2}$, deg

δ_b body-flap deflection angle, positive down, deg

δ_e elevon deflection angle, positive when deflected down, $\frac{\delta_{e,left} + \delta_{e,right}}{2}$, deg

Subscripts:

max maximum

trim trimmed condition

APPARATUS AND TESTS

Tunnels

The Mach 20 tests were conducted in the Langley 22-inch helium tunnel. Operational characteristics of this facility and details of the contoured-nozzle flow characteristics are available in reference 10. The Mach 6 tests were conducted in air in the Langley 20-inch Mach 6 tunnel. The general details of the tunnel along with the schematic drawings and calibration are presented in reference 11.

Models

The unmodified models (called baseline models) shown in figures 1 and 2 were similar to the Martin-Marietta Corporation delta-wing orbiters, presented in reference 12. The model tested at Mach 20 was approximately 18.58 cm in length with a reference area of 91.61 cm^2; the model tested at Mach 6 was 30.5 cm in length with a reference area of 248.39 cm^2. The baseline model was progressively altered for the Mach 20 tests as follows: (1) tip fins removed, elevon span extended to wing tip, and dorsal fin added; and (2) a two-position body flap at -10^o and 0^o with four wing variations including elevon hinge-line sweep angles of 31^o rearward (W_1), 0^o (W_2 and W_3), and 27^o forward (W_4). All the wings were positioned on the body at the same location, and all the elevons were designed to have identical chords (perpendicular to hinge). These alterations are shown in figure 3, and the wing designations and descriptive parameters are presented in the following table:

Wing	Total planform area, cm^2	Span, cm	Trailing-edge sweep angle, deg	Elevon area, cm^2
W_1	91.61	9.90	31 (rearward)	4.53
W_2	85.75	9.75	0	4.07
W_3	91.55	10.31	0	4.28
W_4	88.84	9.44	27 (forward)	4.00

For the Mach 6 tests, a dorsal fin was added and tip fins were removed. (See fig. 4.)

Test Conditions and Methods

All models were mounted on sting-supported six-component strain-gage balances. Because of the limitations of the angle-of-attack mechanism in the helium tunnel, two

stings (one straight and the other bent) were required to cover the complete angle-of-attack range of 0^{o} to 45^{o} at sideslip angles of 0^{o} and 4.5^{o} for the Mach 20 tests. Longitudinal aerodynamic data presented in reference 13 for the same model mounted on various stings showed no effect due to the use of bent stings at high angles. The angles of attack for the Mach 6 tests varied from 0^{o} to 55^{o} at sideslip angles of 0^{o} and -4^{o}.

The angles of attack were set optically by the use of a point source of light and a small lens-prism combination mounted on the model. The image of the source was reflected by the prism and focused by the lens onto a calibrated chart. Additional features of the systems can be found in reference 10 for the Mach 20 tests and in reference 14 for the Mach 6 tests.

The Reynolds numbers, based on model length, were 1.5×10^{6} for the tests at M = 19, 2.9×10^{6} for the tests at M = 20.6, and 4.8×10^{6} for the tests at M = 6. The Mach number - Reynolds number variation at a Mach number near 20 was obtained by changing the stagnation pressure of the tunnel.

The maximum uncertainties for the tests are presented in the following table:

	M ≈ 20	M = 6
C_N	±0.007	±0.007
C_A	±0.002	±0.001
C_m	±0.0008	±0.0006
C_l	±0.0003	±0.0002
C_n	±0.0003	±0.0002
C_Y	±0.002	±0.002
α, deg	±0.1	*0.1
β, deg	*0.1	±0.1
δ_a, δ_b, and δ_e, deg	±0.05	±0.05
M	±0.2	±0.02

The uncertainties in the M ≈ 20 tests were determined from a static calibration of the strain-gage balance, readout errors, and test-section Mach number calibrations. The accuracies for the M = 6 tests were based on a combination of balance calibration and readout and dynamic pressure accuracies and were calculated by the root-mean-square method. Model base pressures were measured and the axial-force component was adjusted to a condition where free-stream static pressure acted over the base area.

RESULTS AND DISCUSSION

Baseline Configuration

The longitudinal aerodynamic characteristics of the baseline configuration (with wing tip fins) are presented in figures 5 and 6 for M = 19 and M = 6, respectively.

The Mach 19 results show that the vehicle had stable trim points at angles of attack of 14^{o} and 35^{o} for a 15^{o} change in elevon deflection. The Mach 6 data show a stable trimmed condition at $\alpha = 45^{o}$ for $\delta_e = -10^{o}$. As expected, the Mach number difference did result in different values of $(L/D)_{max}$ - a value of 2.1 at M = 19 and a value of 2.4 at M = 6. However, the directional stability level was about the same for both Mach numbers (fig. 7) with the vehicle becoming slightly unstable below an angle of attack of 13^{o}.

Configuration Alterations at M = 6

.Dorsal-fin addition.- The addition of a dorsal fin to the baseline configuration (resulting in a vehicle with three tails as shown in fig. 4(a)) was made to improve the directional stability at low angles of attack in anticipation of a subsonic requirement. However, this particular dorsal fin, with approximately the same shape as one of the tip fins, had little effect on either the longitudinal or lateral-directional characteristics (fig. 8) at M = 6. The configuration with a larger dorsal fin was tested at M = 19 without a performance loss also, and the results will be discussed in a subsequent section.

Elevon effectiveness for the configuration with the dorsal fin is presented in figure 9 for elevon deflections from -20^{o} to 10^{o} in 10^{o} increments. Since the dorsal fin tested at M = 6 was completely ineffective, the data in figure 9 can be compared with the M = 19 baseline data in figure 5. A comparison of the pitching-moment results indicates that the center of pressure moves forward with increasing Mach number and a more positive elevon deflection is therefore required to maintain the same trim angle. A similar Mach number effect occurred on a high performance, slender, lifting vehicle reported in reference 15. This effect can be attributed, in part, to a difference in the flow expansion along the lower cambered surface of the vehicles for these extreme Mach number conditions.

Tip-fin removal.- During the Phase B study, investigations revealed that the structural weight requirement for the wing tip fins was greater than the weight of a reaction control system required to control the vehicle without fins. In addition, subsonic tests (ref. 16) indicated that the tip fins caused a rearward concentration of lift which resulted in a negative pitching moment at zero lift. These results led to the evaluation of the configuration without tip fins. Figures 10 and 11 show that tip-fin removal had little effect on longitudinal static stability, longitudinal trim, and effective dihedral; however, $(L/D)_{max}$ did increase by approximately 0.7. As expected, the only detrimental effect was a loss in directional stability.

Configuration Alterations at M = 20.6

Tip fins removed, elevon span extended, and dorsal fin added.- In order to reduce the control deflection required for trim near $(L/D)_{max}$ at high Mach numbers (M = 20.6), the elevon span was extended to the wing tip for the configuration without tip fins (fig. 3(a)).

This configuration was evaluated with and without the dorsal fin shown in the figure. Although the center fin was rather large compared with the one tested at $M = 6$ (compare fig. 3(a) with fig. 4(a)), the longitudinal results in figure 12 show that there was no effect on the data for angles of attack from 22° to 44°. This dorsal fin was also relatively ineffective directionally in this angle-of-attack range (fig. 13). Similar effects were obtained for the smaller fin at $M = 6$ over a greater angle-of-attack range (fig. 8).

Elevon hinge-line and wing trailing-edge sweep altered. - The longitudinal aerodynamic characteristics of the four modified wings shown in figure 3(b) are presented in figures 14 to 17 for different elevon and body-flap deflections. All the wings except wing W_1 were tested without the dorsal fin. However, the fin has been previously shown to have a negligible effect on the longitudinal characteristics for the test angle-of-attack range (22° to 44°).

A summary of the wing-shape and elevon hinge-line sweep effects on the trimmed L/D values and the elevon deflections required for trim is shown in figure 18. The extreme angles of attack associated with the trimmed elevon deflections were obtained by extrapolating the pitching-moment data where required. Similar adjustments were not applied to the $(L/D)_{trim}$ data. There was no apparent effect of the wing shape on the trimmed L/D values. The difference between the L/D values approaching the maximum values for the modified wings and the baseline wing can be attributed to the tip fins being on the baseline vehicle (also shown by the $M = 6$ results in fig. 10).

The effect of extending the elevon span to the wing tips can be observed in the bottom plot of figure 18 by the difference in slope of the curve representing the baseline configuration and the curve for the configuration with wing W_1. The two curves are expected to merge near $(\delta_e)_{trim} = -10^{\circ}$ and $\alpha = 40^{\circ}$ because the tip fins on the baseline wing are ineffective at this attitude and, since the elevons are flush with the lower surface, their spans are irrevelant. The apparently small influence of the tip fins on the trim angle of attack was also observed at $M = 6$ in figure 10.

The large differences in the required trimmed elevon deflections for the wings W_2 and W_3 (both with unswept trailing edges) can be attributed to the difference in the location of the elevon relative to the vehicle center-of-gravity location. (See fig. 3(b).) Wing W_3 required less positive deflections because its elevon trailing edge extended beyond the vehicle base which resulted in a longer moment arm. Wing W_4 (trailing edge swept forward) had acceptable elevon deflections, 5° to -5°, for trim angles of attack from 19° to 53°.

The effect of roll control on the yawing moment was studied by differentially deflecting the elevons on the four modified wings 5° from the deflections required for longitudinal trim at two general angles of attack. One trim angle was approximately 20°, which is near the angle of attack for $(L/D)_{max}$, and the other was near 47°, which approaches the angle

of attack for $C_{L,max}$. The longitudinal data for these two trim conditions are shown in figures 19 to 22, and the pertinent elevon deflections are given in the following table:

Wing	δ_e, deg	α_{trim}, deg	$C_{n_{\delta_a}}/C_{l_{\delta_a}}$
W_1	0	21	-0.34
	-10	46	-.32
W_2	7	20	-0.33
	3	47	-.41
W_3	0	20	-0.18
	-12.5	46	-.05
W_4	5	20	-0.09
	-5	50	-.01

Wing W_1 had a body-flap deflection angle of -10°, and this angle was 0° for the other wings.

The lateral-directional results in figure 23 show that adverse yaw due to roll control occurred for all elevon hinge-line sweep angles studied. The magnitude of the cross coupling produced by the ailerons for the different wings is indicated in the above table where the values for the ratio $C_{n_{\delta_a}}/C_{l_{\delta_a}}$ are given for the low and high longitudinal trim angles of attack. The results show that by unsweeping the elevon hinge line with the trailing edge at the body base (wing W_2) the cross coupling was the same order of magnitude as that for wing W_1. Extending the unswept elevons beyond the body base (wing W_3) resulted in a reduction of the cross coupling at both trim-angle conditions. This improvement indicates that the roll-yaw cross coupling can be minimized for unswept trailing edges by decreasing the amount the elevon deflects into the flow. The cross coupling can be further reduced by sweeping the hinge line forward (wing W_4). This additional improvement indicates that the cross coupling can be reduced by directing the resultant forces acting on the elevons toward the center-of-gravity location of the vehicle.

CONCLUDING REMARKS

Experimental longitudinal, lateral, and directional aerodynamic characteristics of a blended delta wing-body entry vehicle have been obtained at Mach numbers near 20 in helium for Reynolds numbers, based on model length, of 1.5×10^6 and 2.9×10^6 and at Mach 6 in air for a Reynolds number, based on model length, of 4.8×10^6. The angles of attack varied from 0° to 55° for two sideslip angles. The study included the effects on a baseline vehicle due to the addition of dorsal fins, the removal of wing tip fins, an increase in elevon size, and changes in elevon hinge-line sweep angle.

The results showed that the baseline vehicle had a maximum lift-drag ratio of 2.1 at Mach 19 and of 2.4 at Mach 6 with about the same lateral and directional stability at both Mach numbers. As Mach number increased from 6 to 20, the longitudinal center of pressure moved forward and a more positive elevon deflection was therefore required to maintain a given trim angle. The removal of wing tip fins from the baseline vehicle increased the maximum lift-drag ratio and had a negligible effect on longitudinal stability, but caused directional instability that could not be eliminated by the dorsal fins examined. The yaw due to roll control was minimized for wings having unswept trailing edges with controls that required little or no positive control deflections and for wings with control surfaces swept forward that directed the resultant control forces toward the center-of-gravity location of the vehicle.

Langley Research Center,
National Aeronautics and Space Administration,
Hampton, Va., July 28, 1972.

REFERENCES

1. Mueller, George E.: The New Future for Manned Spacecraft Developments. Astronaut. & Aeronaut., vol. 7, no. 3, Mar. 1969, pp. 24–32.

2. Clauser, Francis H.: No Law Says Space Must Be Expensive. Astronaut. & Aeronaut., vol. 7, no. 5, May 1969, pp. 32–38.

3. Tischler, A. O.: A Commentary on Low-Cost Space Transportation. Astronaut. & Aeronaut., vol. 7, no. 8, Aug. 1969, pp. 50–64.

4. Mueller, George E.: An Integrated Space Program for the Next Generation. Astronaut. &Aeronaut., vol. 8, no. 1, Jan. 1970, pp. 30–51.

5. Tischler, A. O.: Defining a Giant Step in Space Transportation. Astronaut. & Aeronaut., vol. 9, no. 2, Feb. 1971, pp. 22–25.

6. Faget, Max: Space Shuttle: A New Configuration. Astronaut. & Aeronaut., vol. 8, no, 1, Jan. 1970, pp. 52–61.

7. Quest, Roland; and Waganer, Lester M.: A Shuttle To Fit the Times. Astronaut. & Aeronaut., vol. 8, no. 8, Aug. 1970, pp. 36–45.

8. Draper, Alfred C.; Buck, Melvin L.; and Goesch, William H.: A Delta Shuttle Orbiter. Astronaut. & Aeronaut., vol. 9, no. 1, Jan. 1971, pp. 26–35.

9. Henderson, Arthur, Jr.: Technology for Aerothermodynamics. Astronaut. & Aeronaut., vol. 9, no. 2, Feb. 1971, pp. 26–36.

10. Arrington, James P.; Joiner, Roy C., Jr.; and Henderson, Arthur, Jr.: Longitudinal Characteristics of Several Configurations at Hypersonic Mach Numbers in Conical and Contoured Nozzles. NASA TN D-2489, 1964.

11. Goldberg, Theodore J.; and Hefner, Jerry N. (With appendix by James C. Emery): Starting Phenomena for Hypersonic Inlets With Thick Turbulent Boundary Layers at Mach 6. NASA TN D-6280, 1971.

12. Anon.: A Two-Stage Fully Reusable Space Transportation System. M-69-19, Martin-Marietta Corp., Sept. 15, 1969.

13. Arrington, James P.; and Woods, William C.: Hypersonic Aerodynamics and Entry-Maneuver—Aerothermodynamic Interactions for Two Lifting Entry Vehicles. NASA TN D-6753, 1972.

14. Ashby, George C., Jr.; and Staylor, W. Frank: Aerodynamic Characteristics of a Modified Cone—Conical-Frustum Entry Configuration at Mach 6.0. NASA TN D-4598,1968.

15. Arrington, James P.; and Ashby, George C., Jr.: Hypersonic Aerodynamic Characteristics Associated With the Evolution of an Entry Configuration With Maximum Lift-Drag Ratio of 3. NASA TM X-2090, 1970,

16. Freeman, Delma C., Jr.: Effect of Configuration Modifications on the Low-Subsonic Aerodynamic Characteristics of a Space Shuttle-Orbiter Concept With a Blended Delta Wing-Body. NASA TM X-2513, 1972.

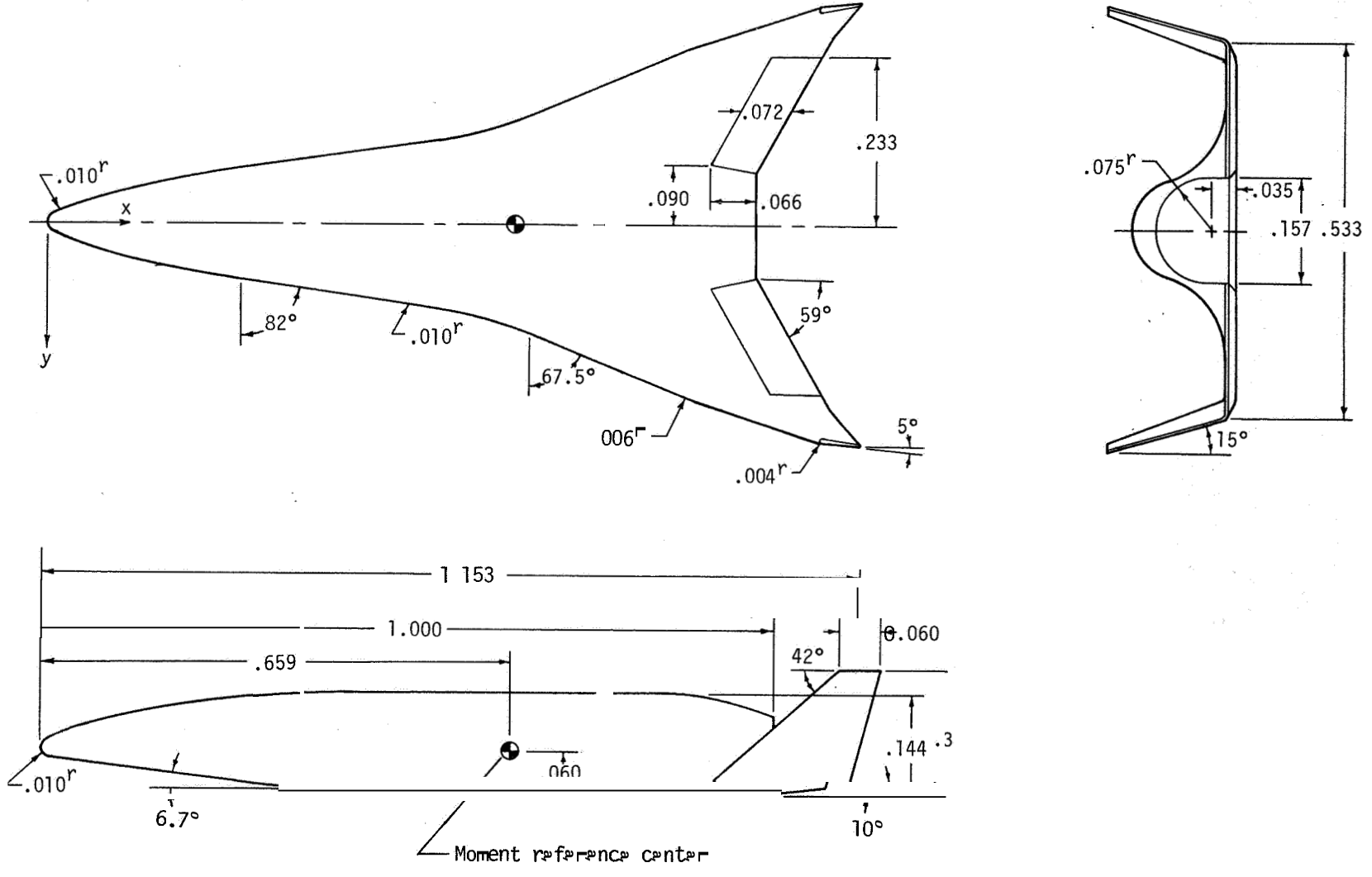

Figure 1.- Baseline configuration shown with $\delta_e = -10^o$. All dimensions have been normalized by the body length ($\ell = 18.58$ cm for $M \approx 20$ tests and $\ell = 30.5$ cm for $M = 6$ tests).

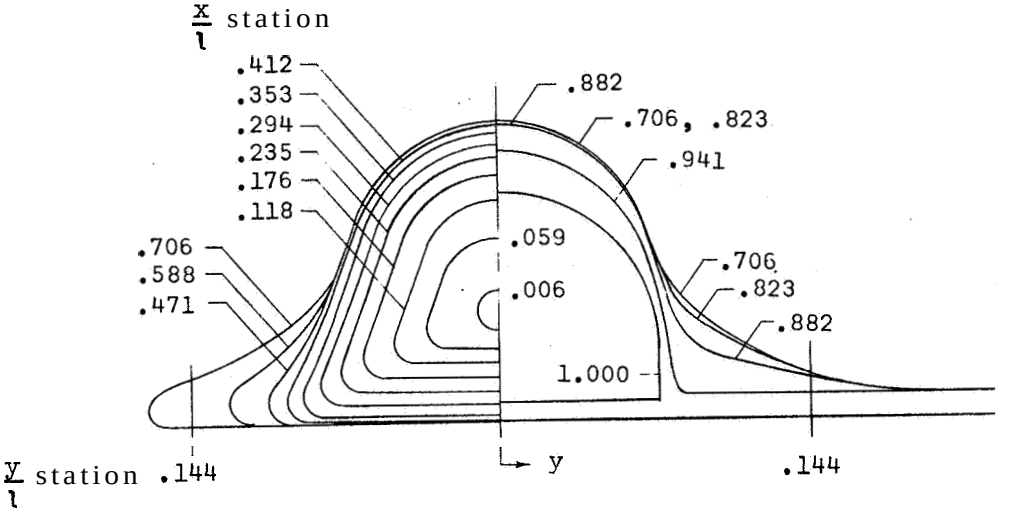
x/l station
.412
.353
.294
.235
.176
.118
.706
.588
.471
.882
.706, .823
.941
.059
.006
1.000
.706
.823
.882
y/l station .144
y
.144

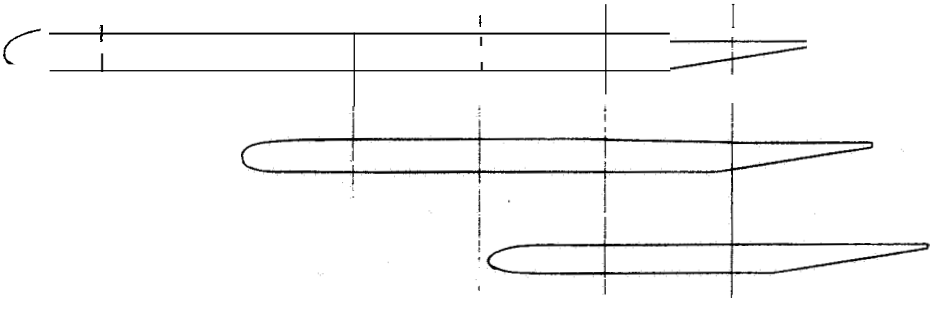
I
.144

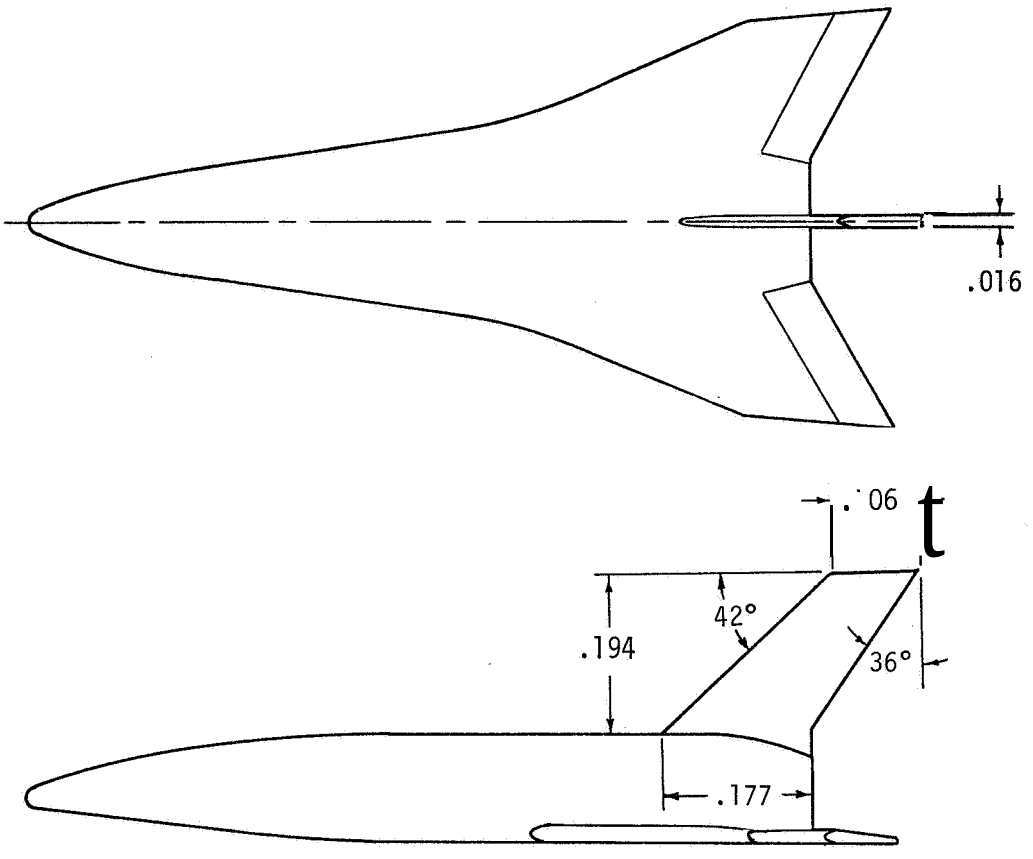

(a) Wing tip fins removed, elevon span extended, and dorsal fin added.

Figure 3.- Model alterations for the $M \approx 20$ tests. Dimensions have been normalized by the body reference length (ℓ = 18.58 cm). $\delta_e = 0^o$ shown.

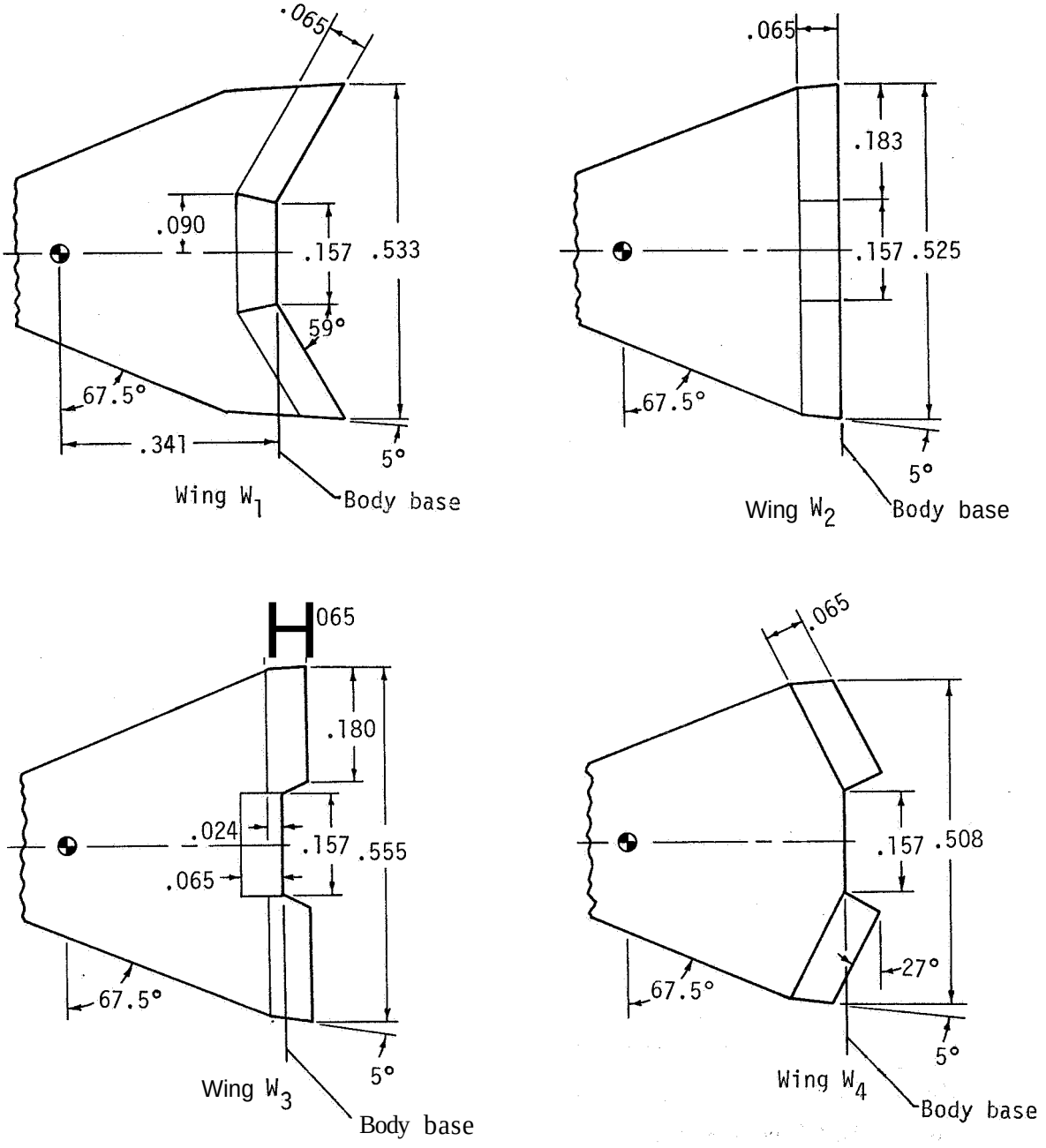

(b) Wing-elevon variations and a body flap added.

Figure 3.- Concluded.

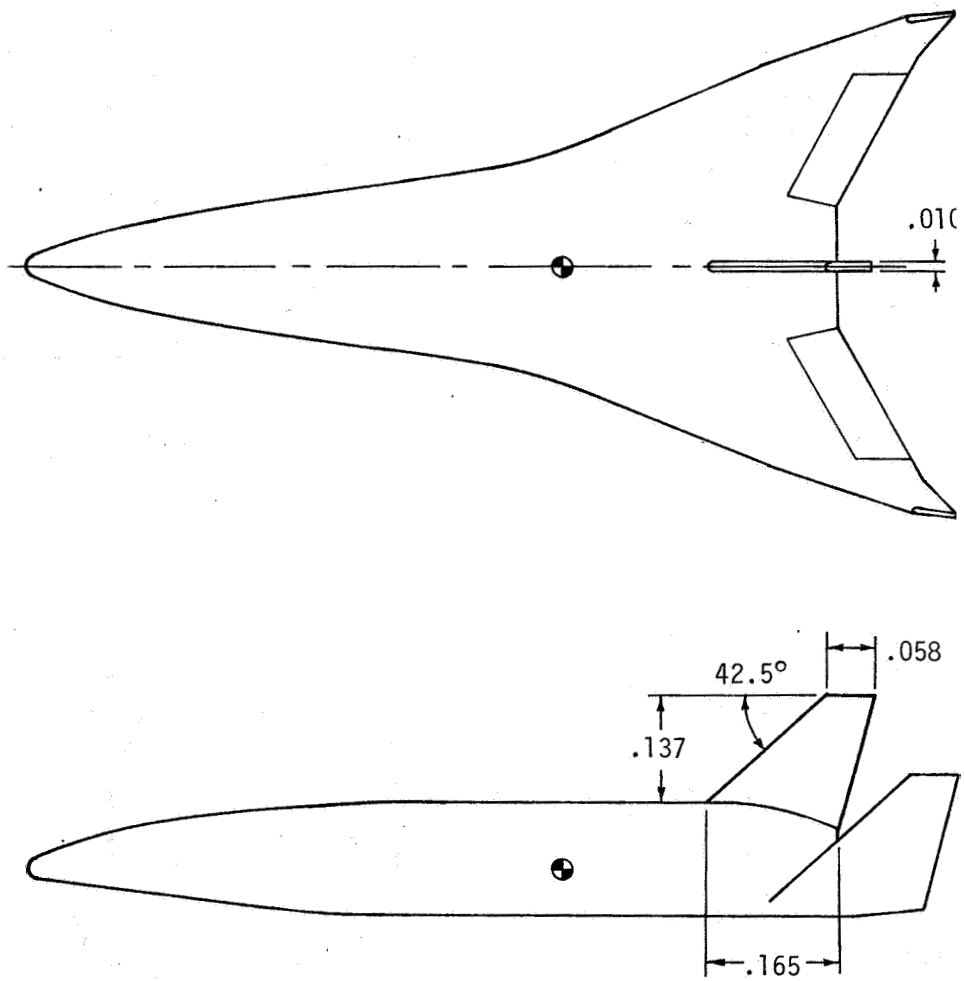

(a) Dorsal **fin added to baseline.**

Figure 4.- Model alterations for M = 6 tests. Dimensions have been normalized by the body length (ℓ = 30.5 cm). $\delta_e = -10^o$ shown.

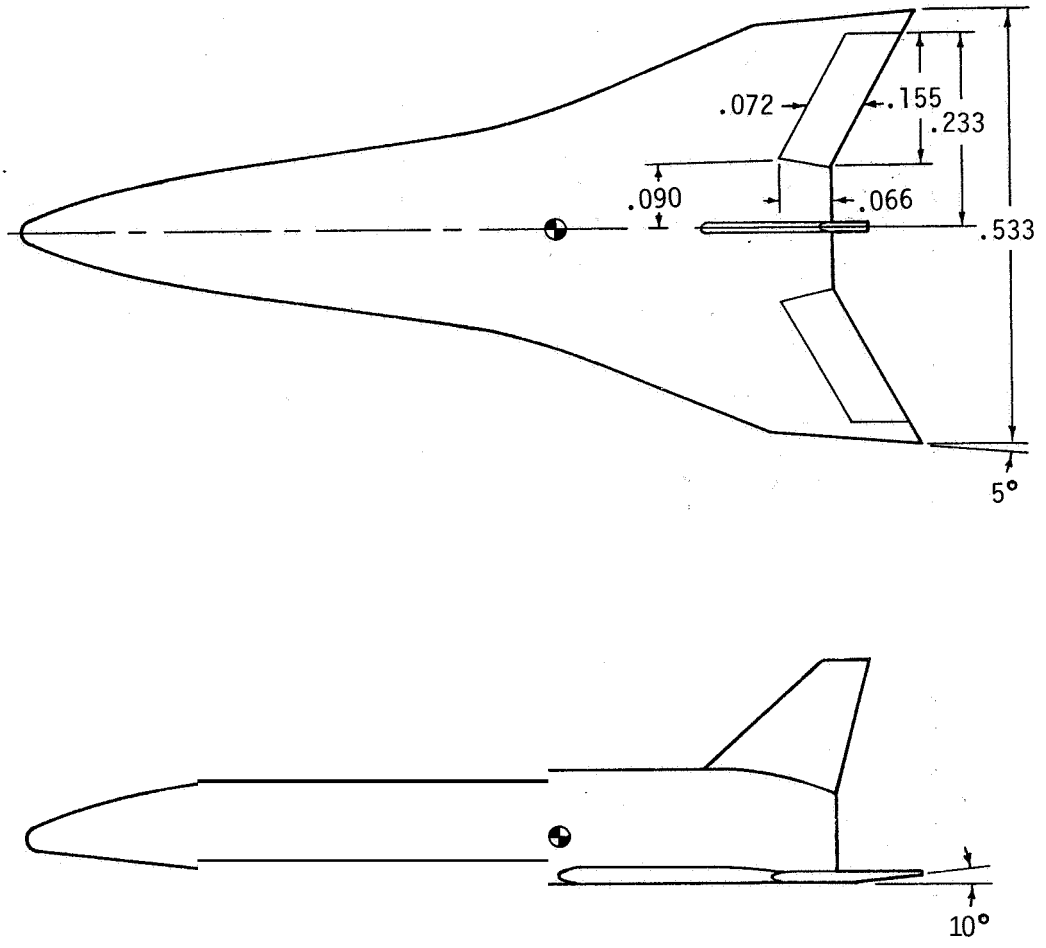

(b) Wing tip fins removed and dorsal fin added. Note that the elevon span was not changed. $\delta_e = -10^{\circ}$ shown.

Figure 4.- Concluded.

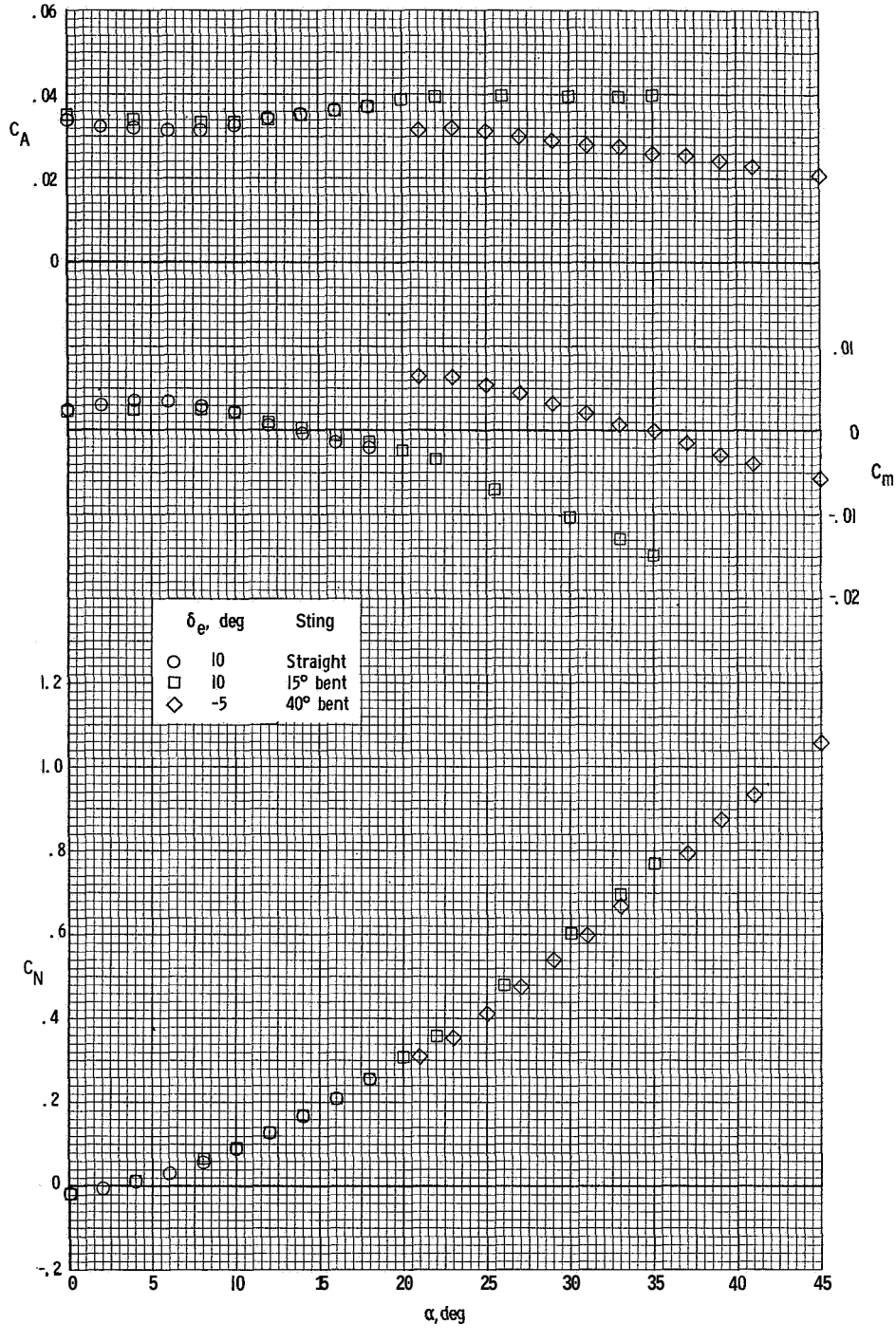

Figure 5.- Effect of elevon deflections on the longitudinal aerodynamic characteristics of the baseline configuration at M = 19 and R = 1.5×10^6.

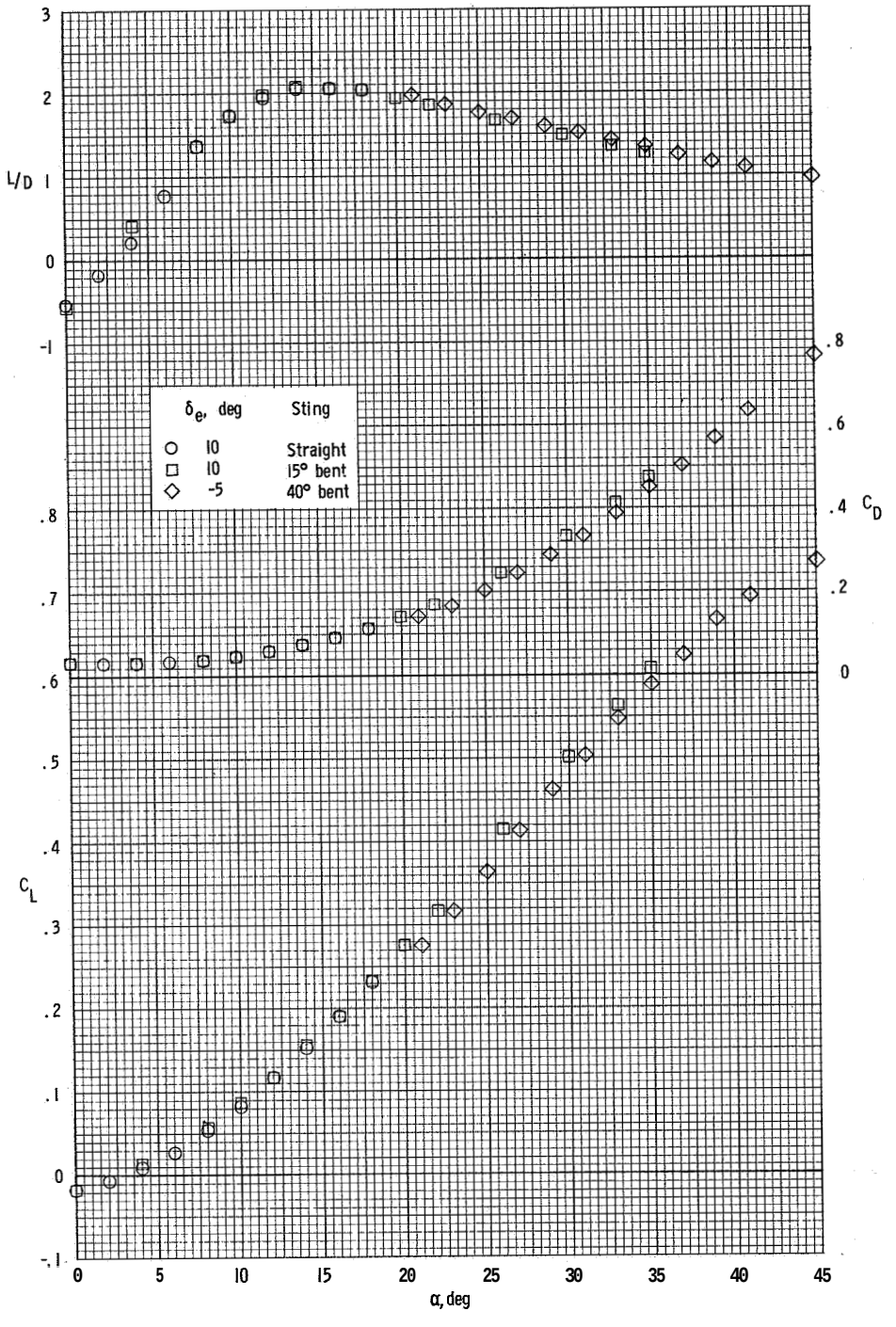

Figure 5. - **Concluded.**

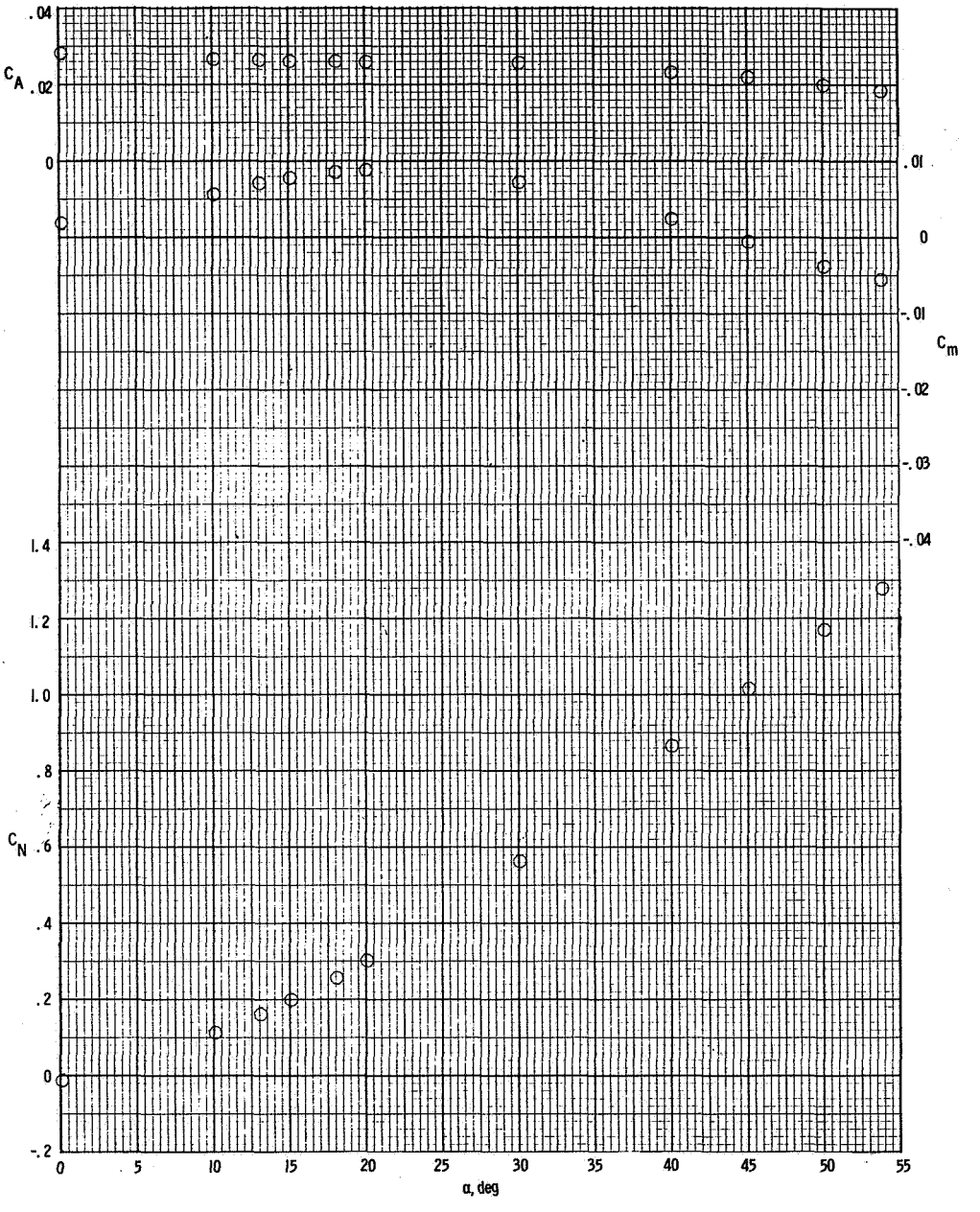

Figure 6.- Longitudinal aerodynamic characteristics of the baseline configuration with $\delta_e = -10^{\circ}$ at M = **6** and R = **4.8** $\times 10^6$.

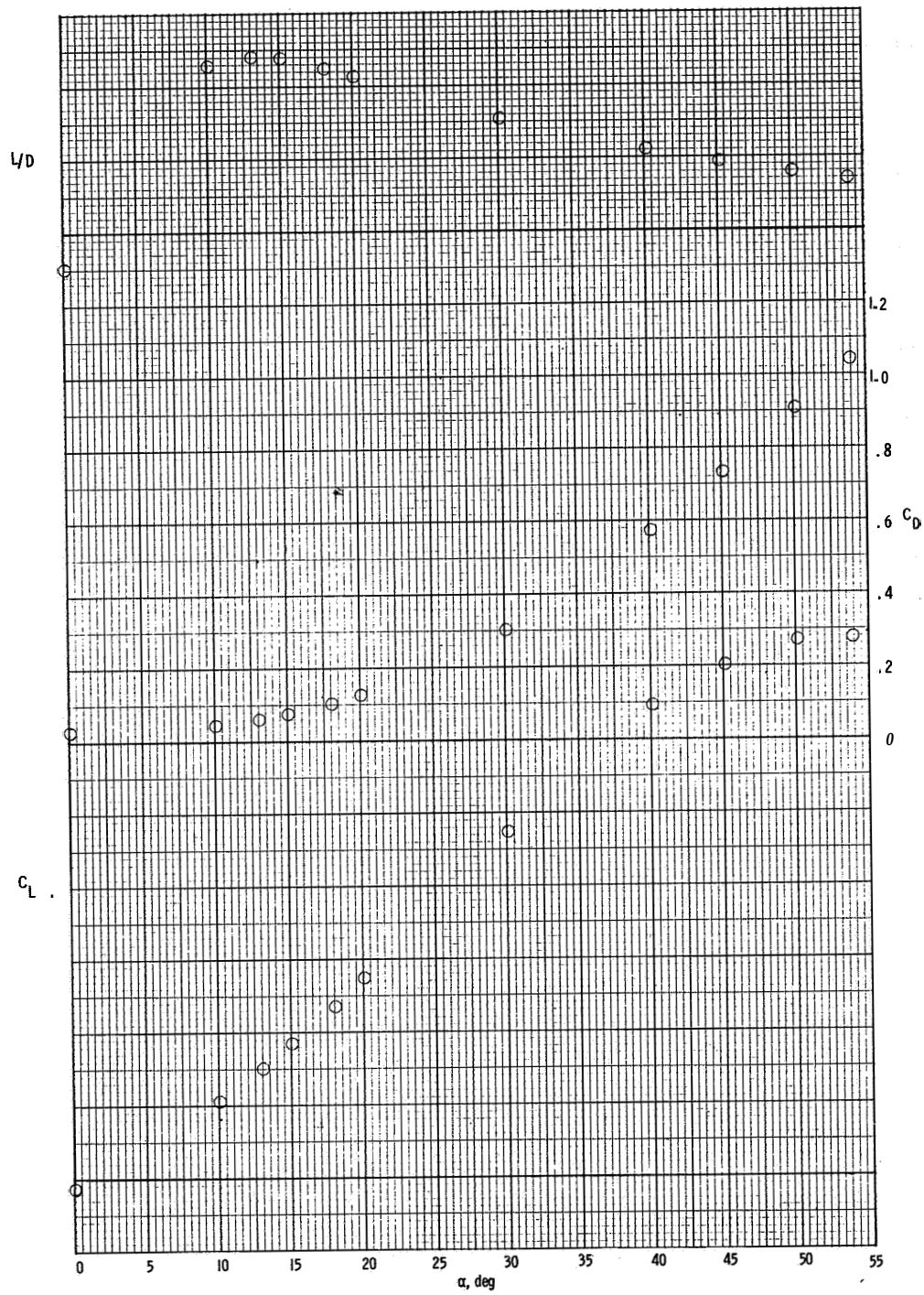

Figure 6. - Concluded.

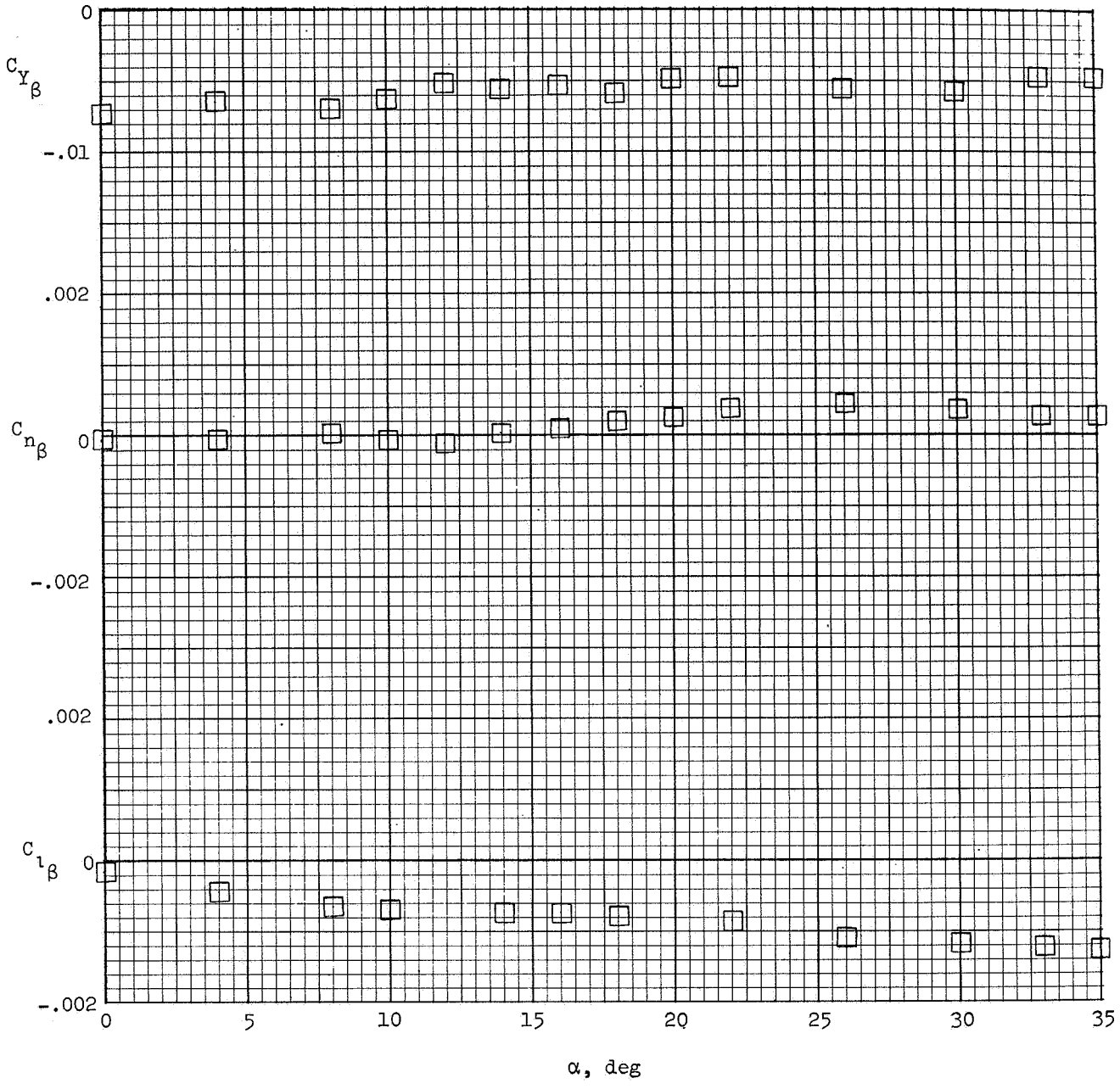

(a) M = 19; $R = 1.5 \times 10^6$; $\delta_e = 10^o$.

Figure 7.- Lateral and directional aerodynamic stability derivatives for the baseline configuration.

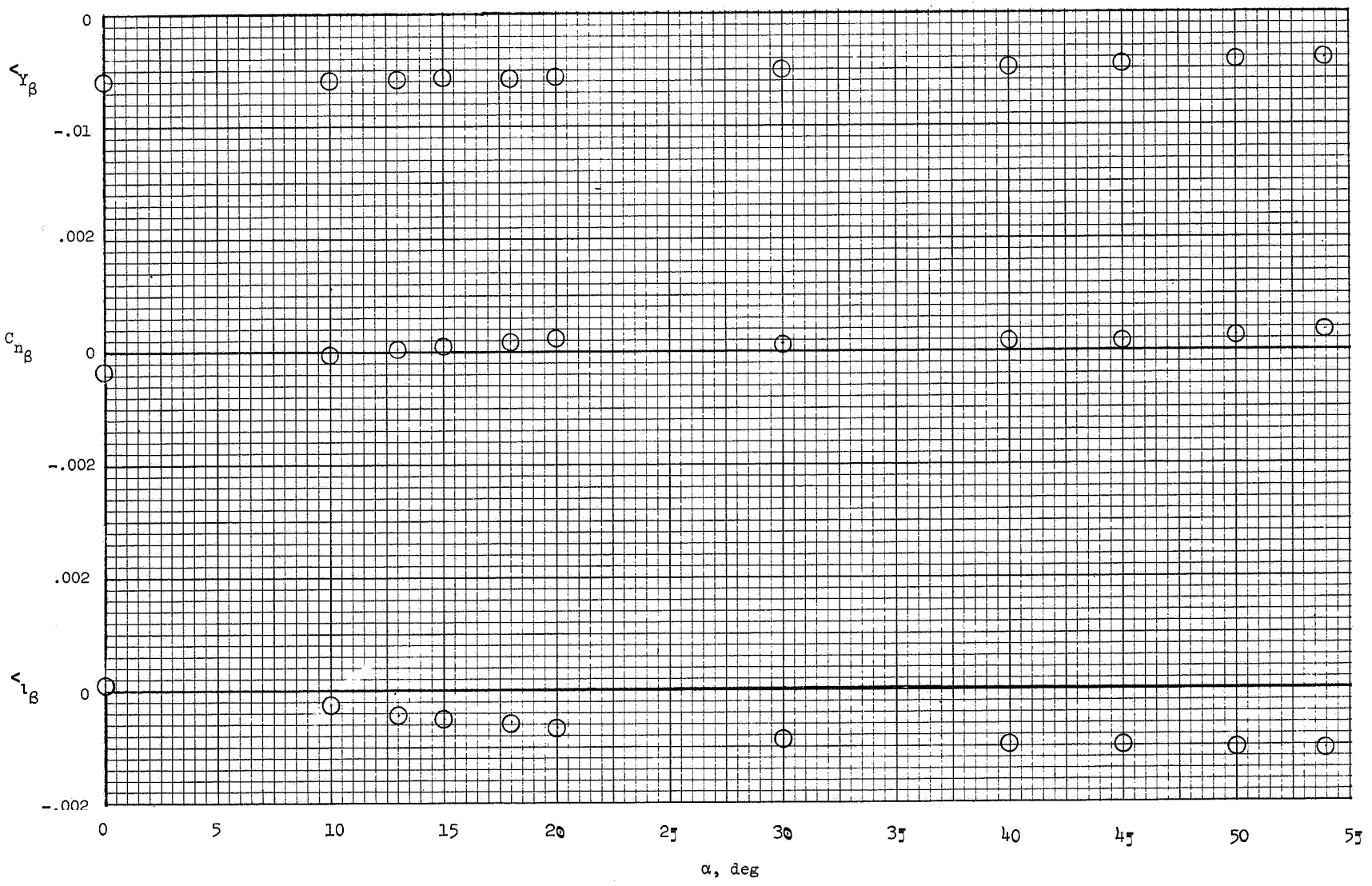

(b) M = 6; R = 4.8×10^6; $\delta_e = -10^o$.

Figure 7.- Concluded.

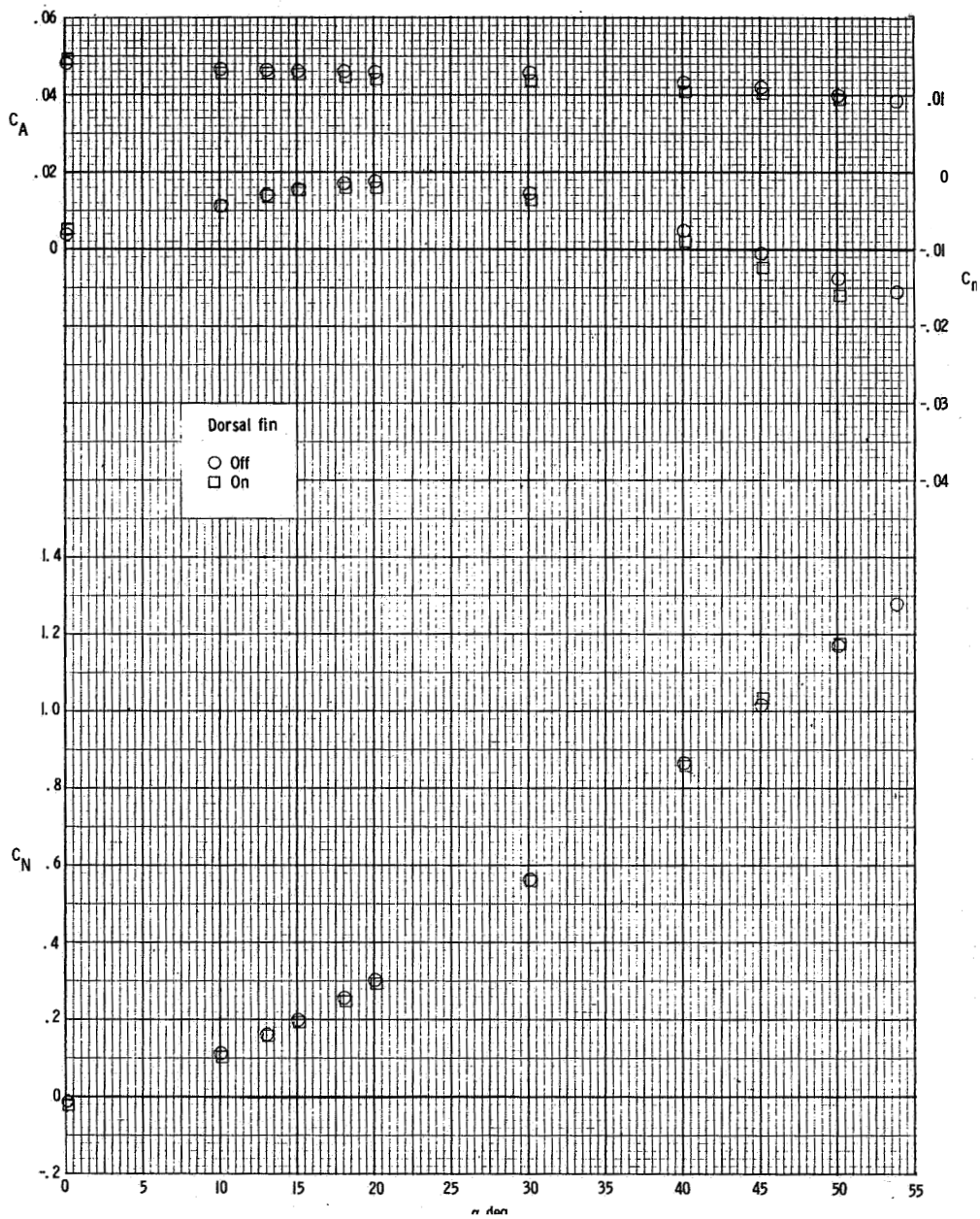

Figure 8.- Effect of dorsal-fin addition on the aerodynamic characteristics of the baseline configuration at $M = 6$ and $R = 4.8 \times 10^6$ with $\delta_e = -10^\circ$.

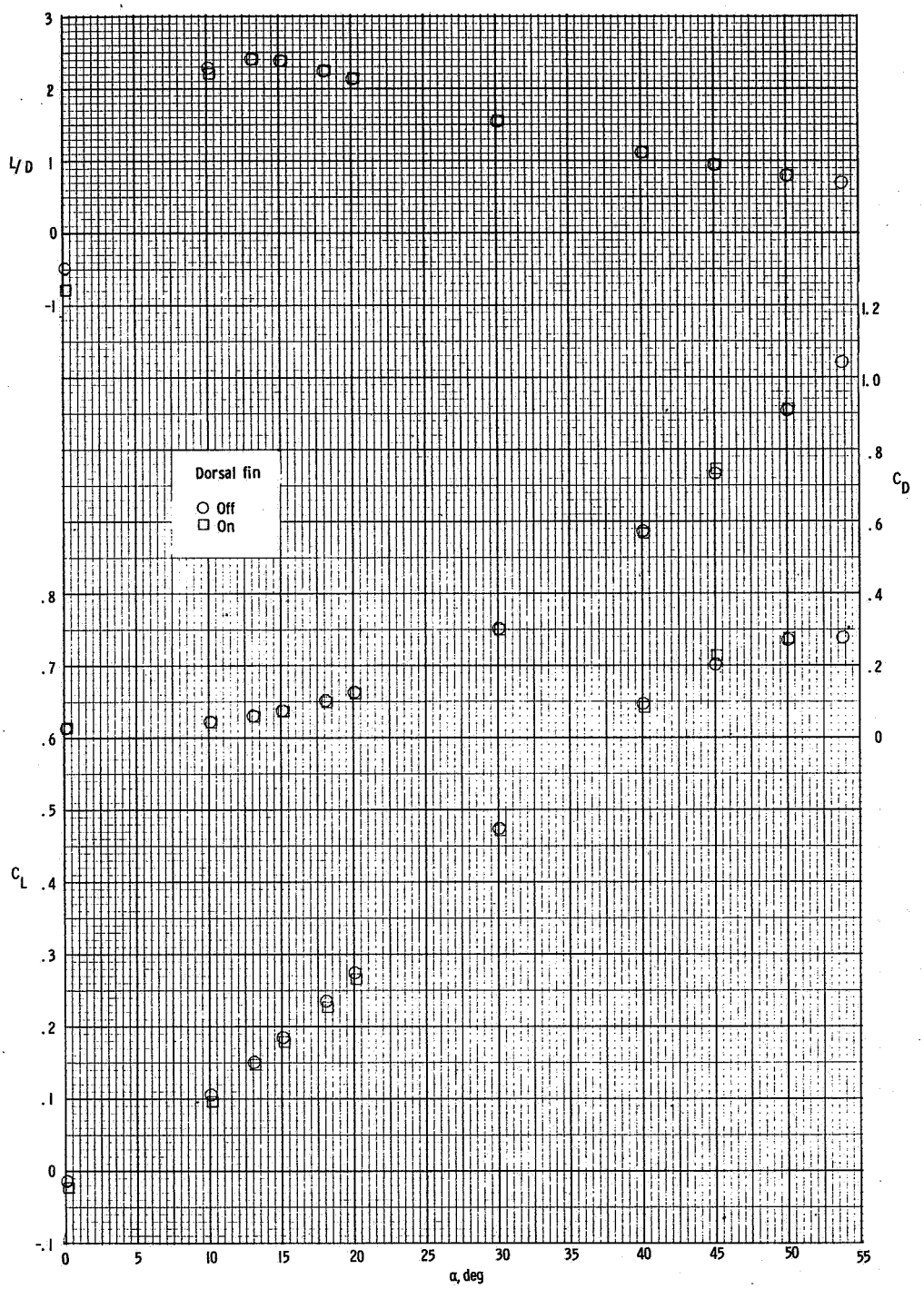

Figure **8.** - Continued.

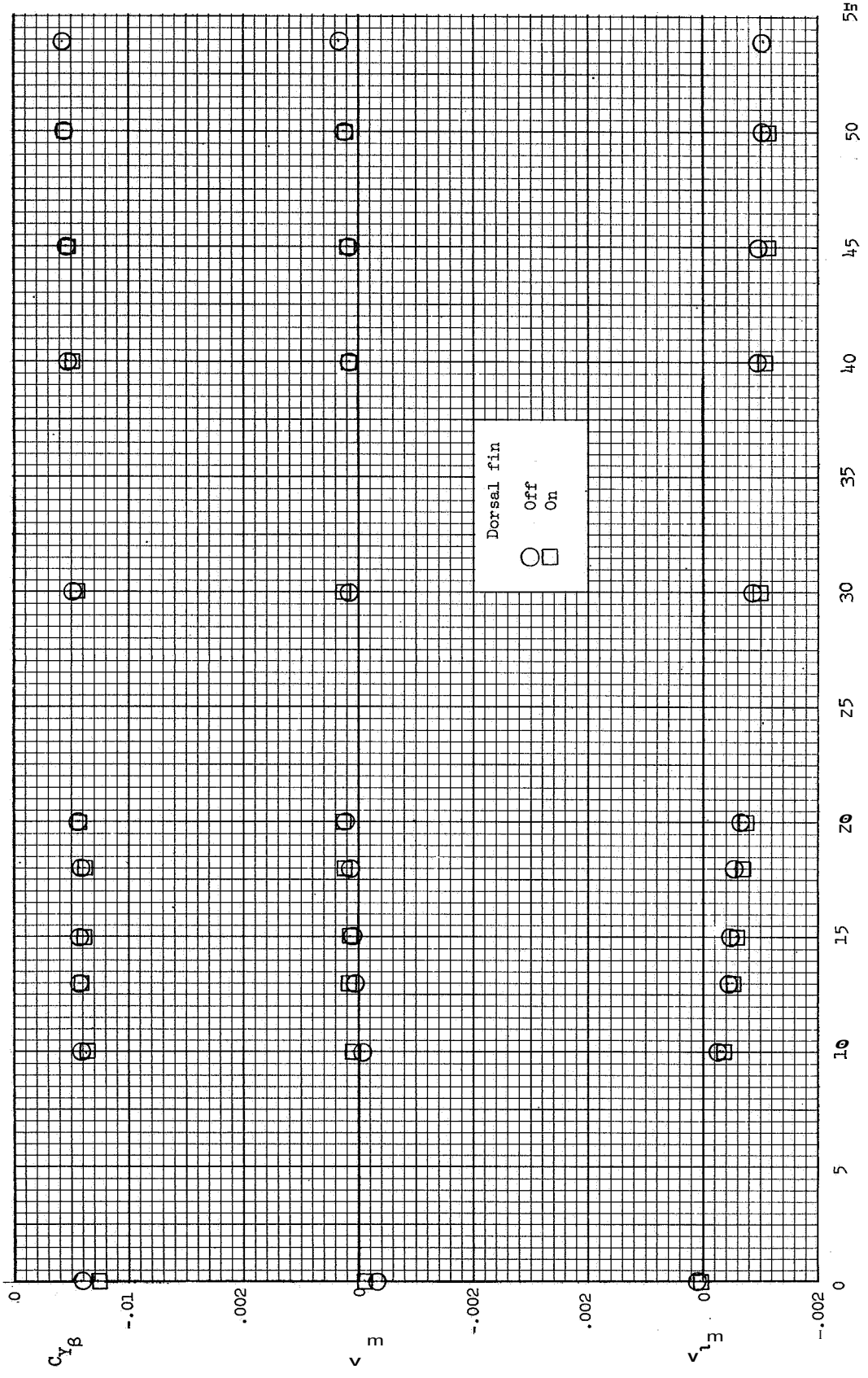

Figure 8.- Concluded.

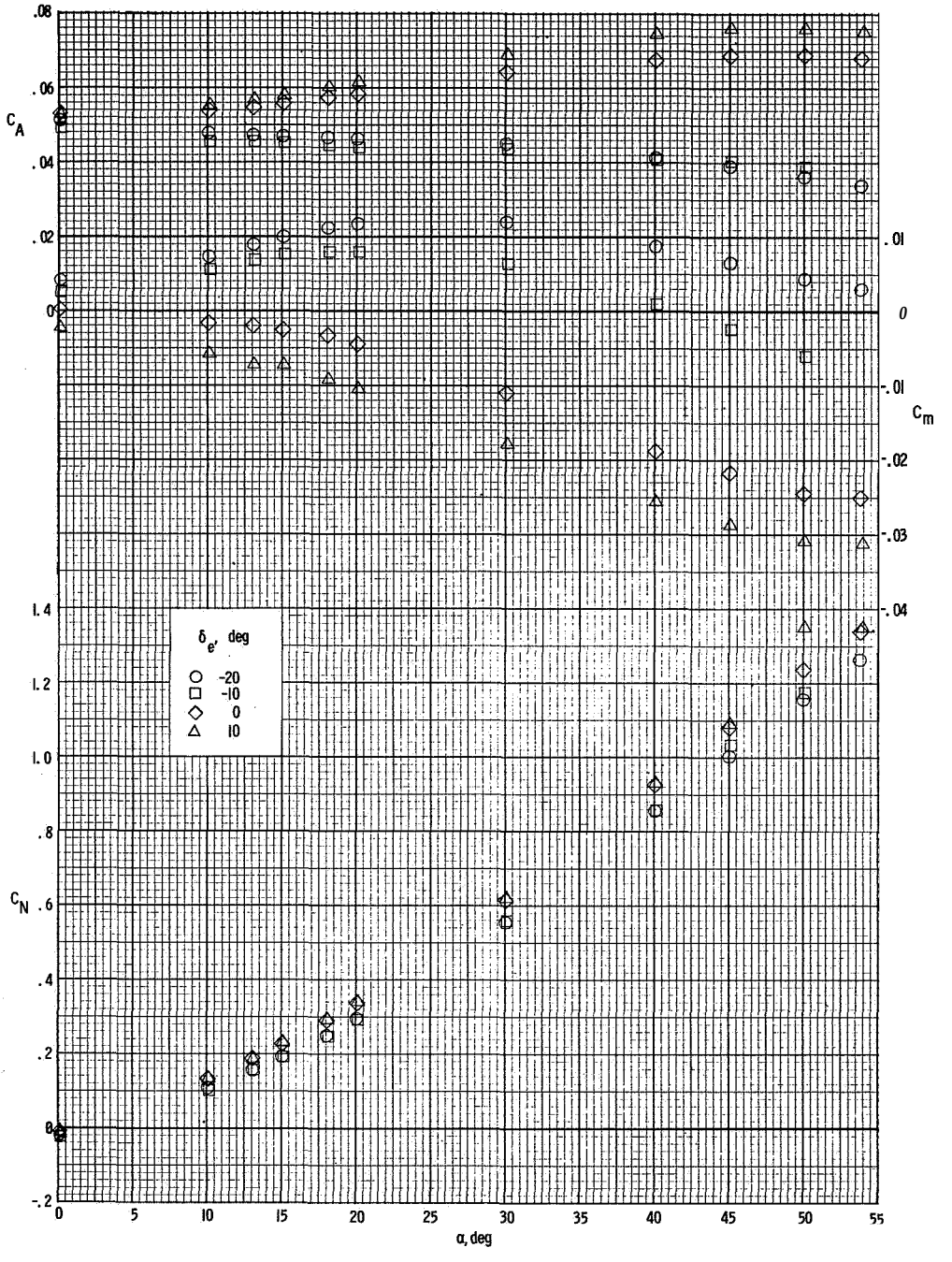

Figure 9.- Effect of elevon deflections on the aerodynamic characteristics of the baseline configuration with a dorsal fin at $M = 6$ and $R = 4.8 \times 10^6$.

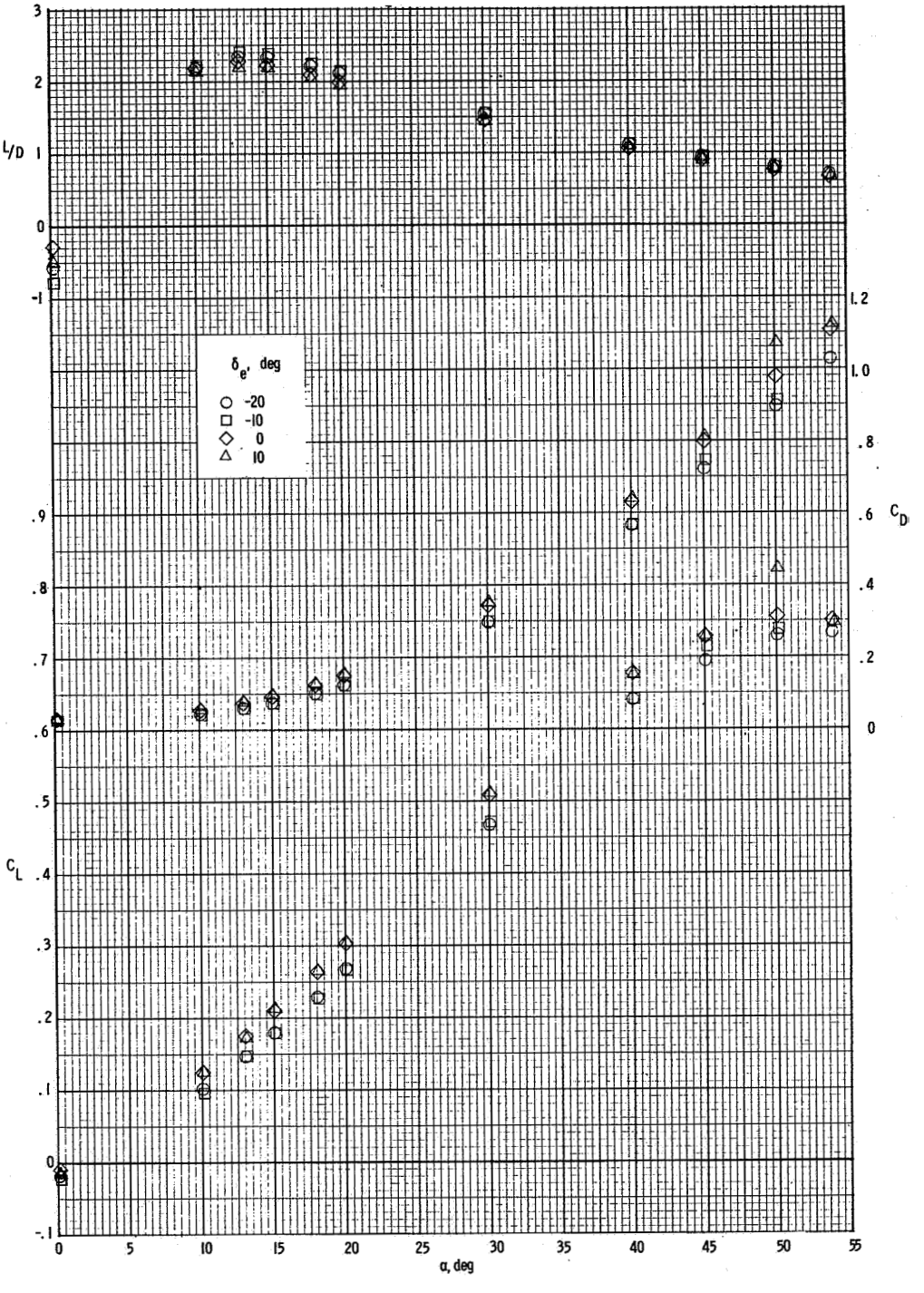

Figure 9.– Continued.

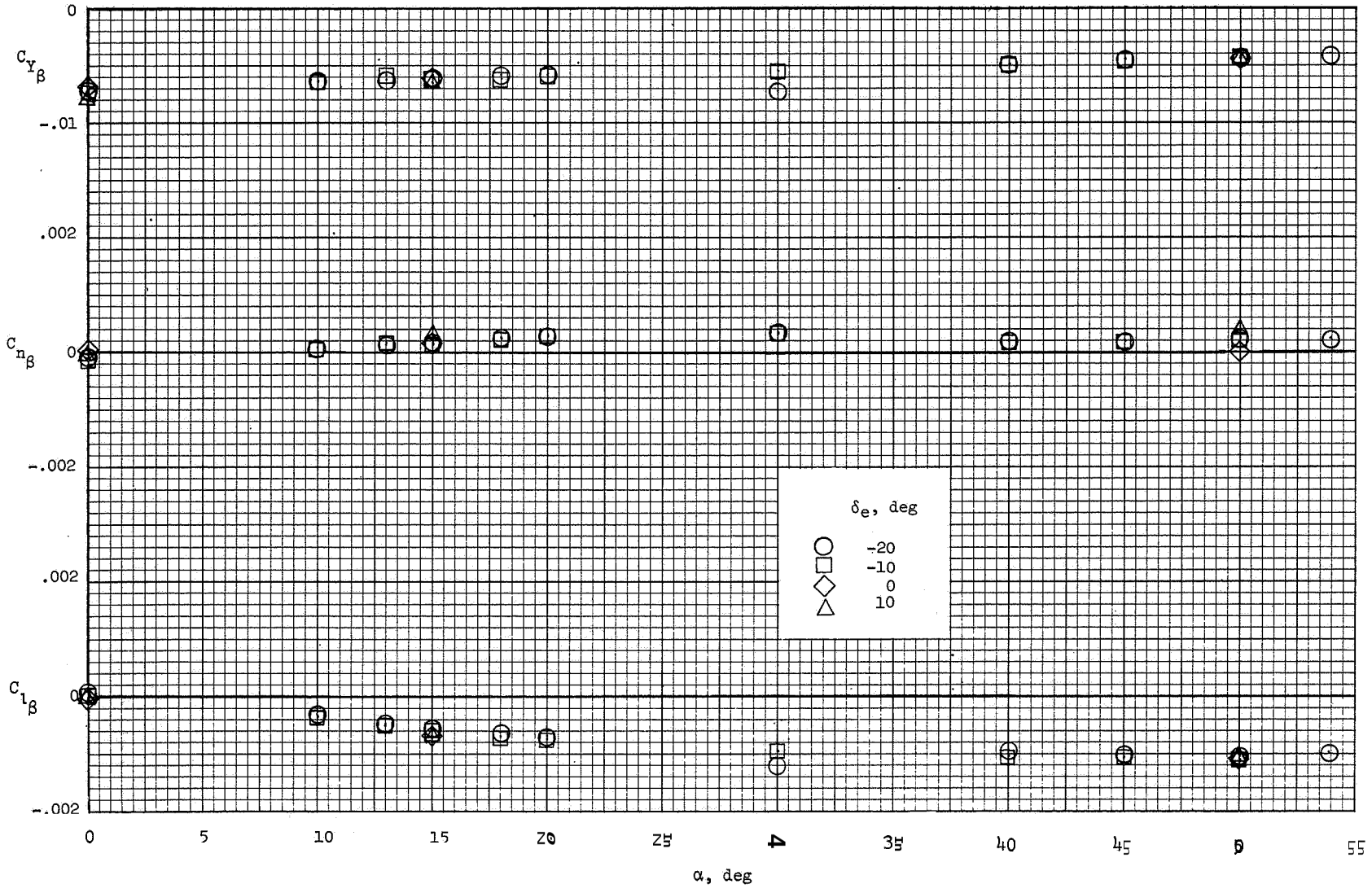

Figure 9.- Concluded.

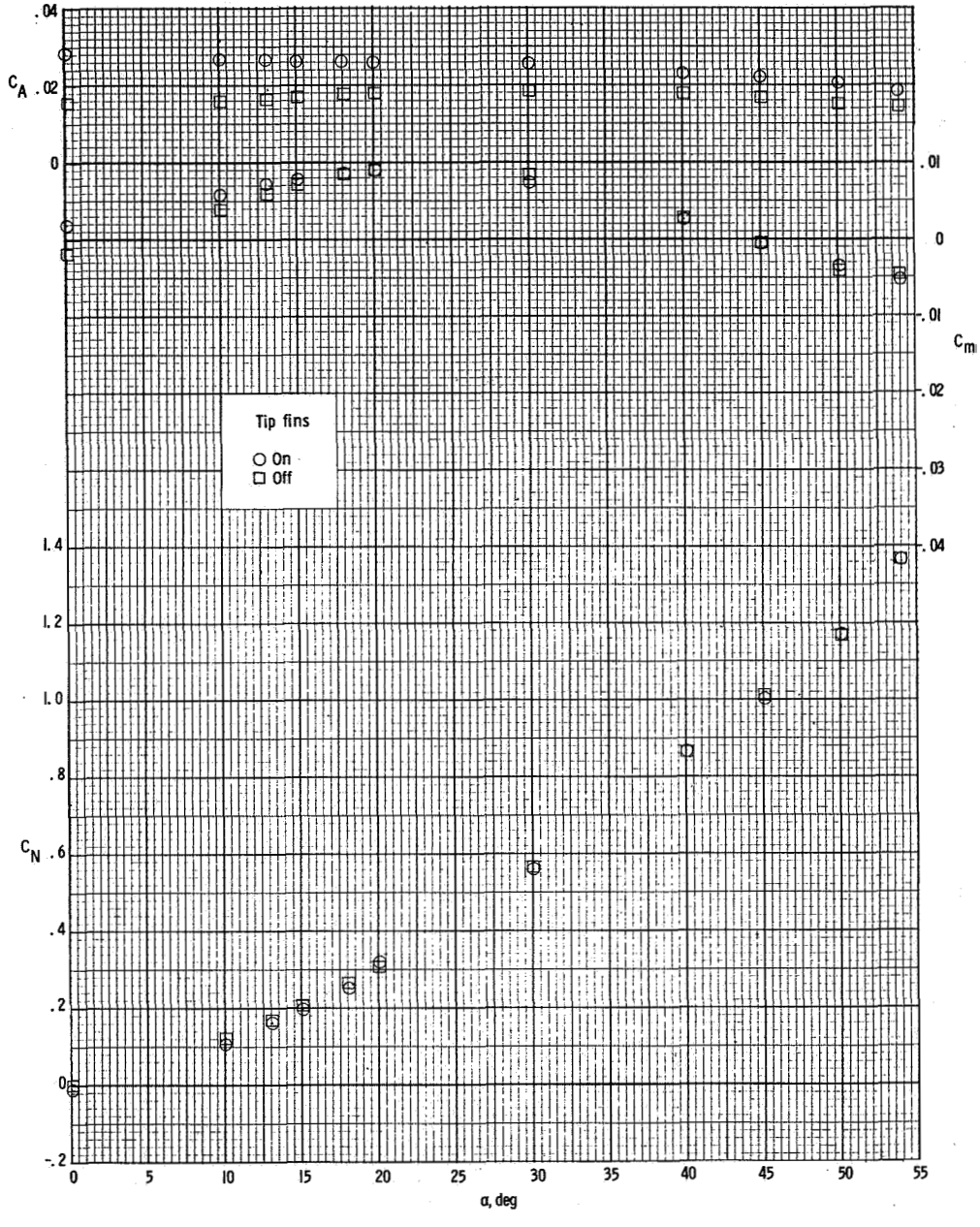

Figure 10.- Effect of tip-fin removal on the aerodynamic characteristics of the baseline configuration at M = 6 and $R = 4.8 \times 10^6$ for $\delta_e = -10^o$.

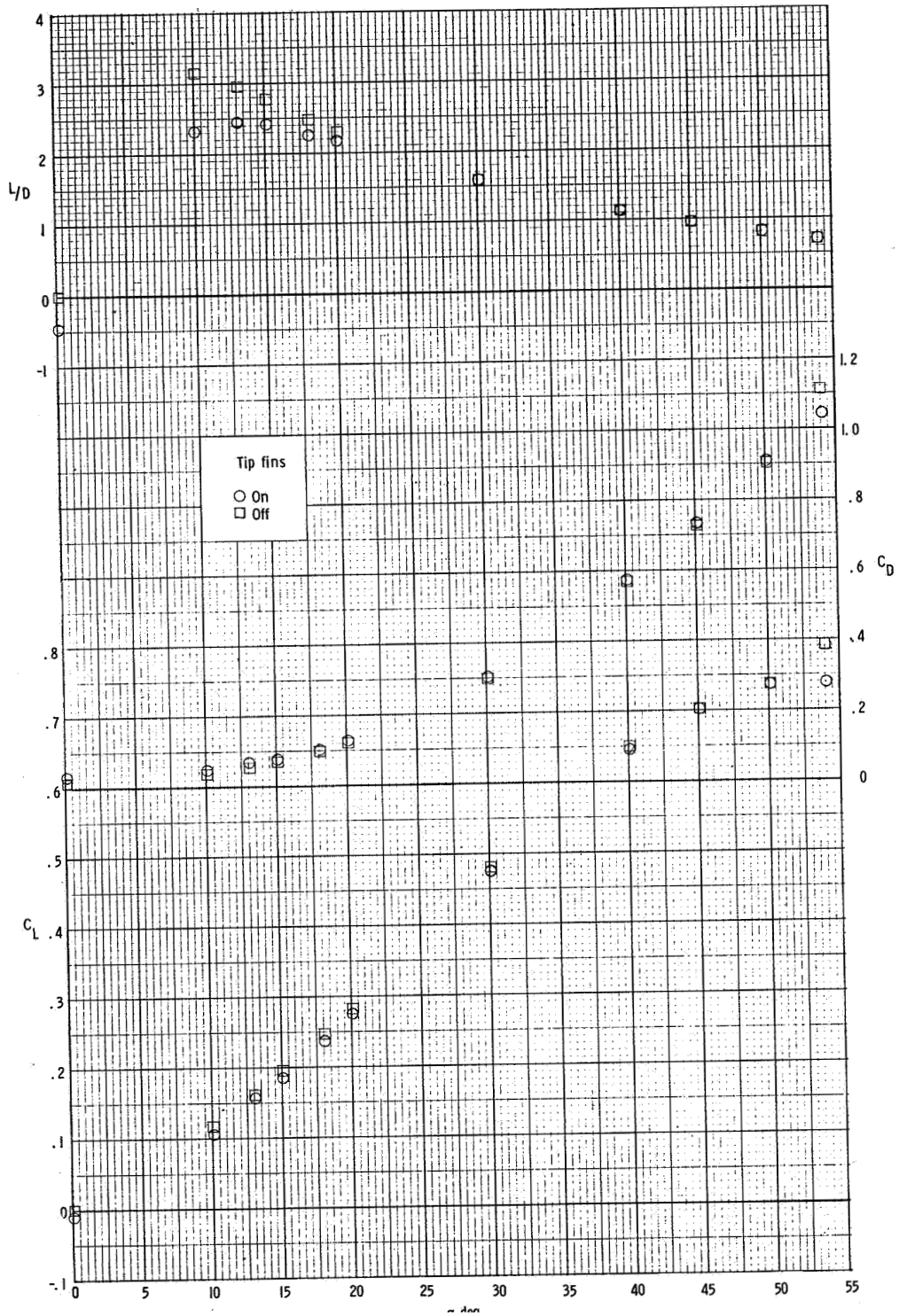

Figure 10.- Continued.

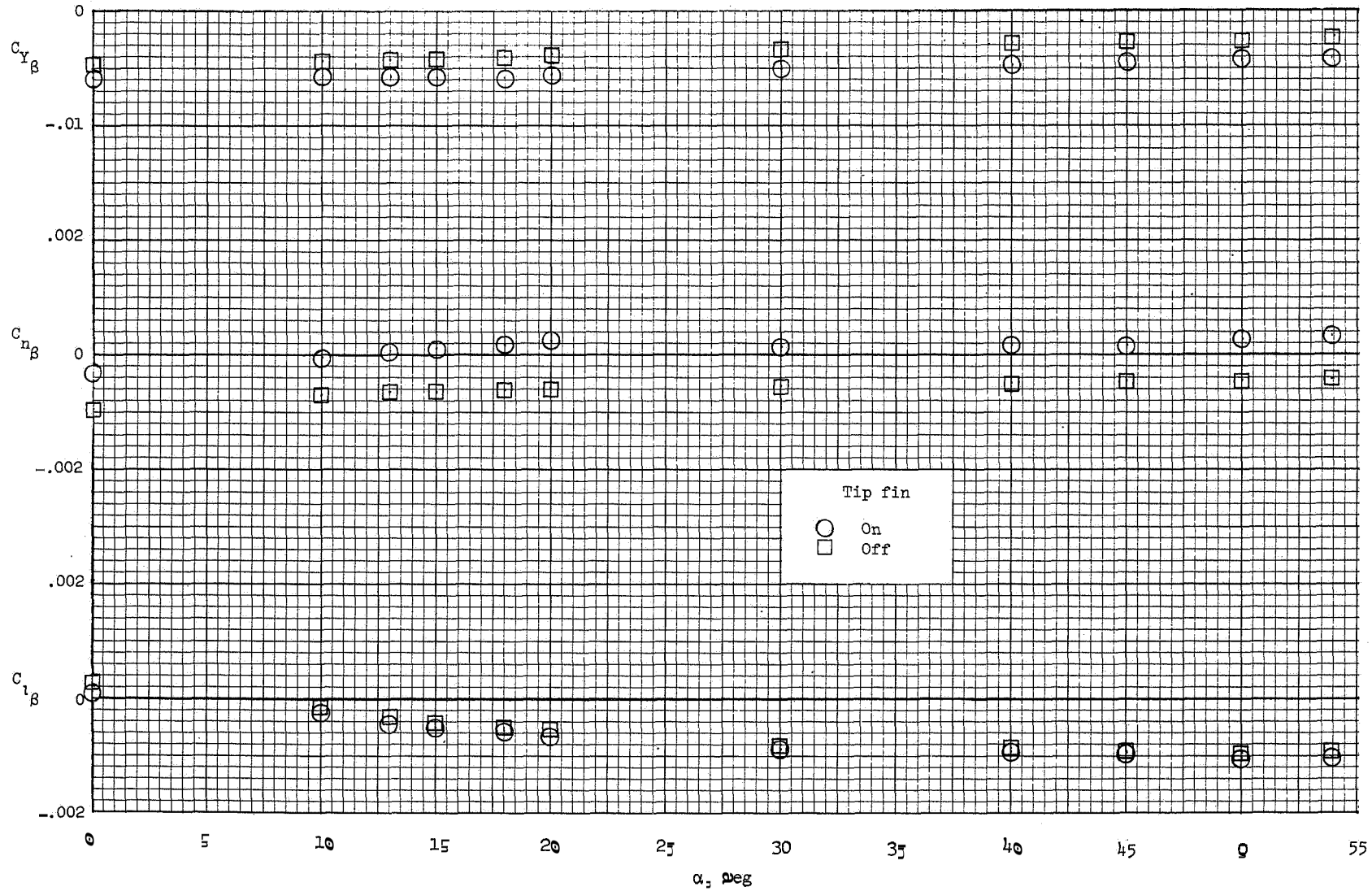

Figure 10 - Concluded.

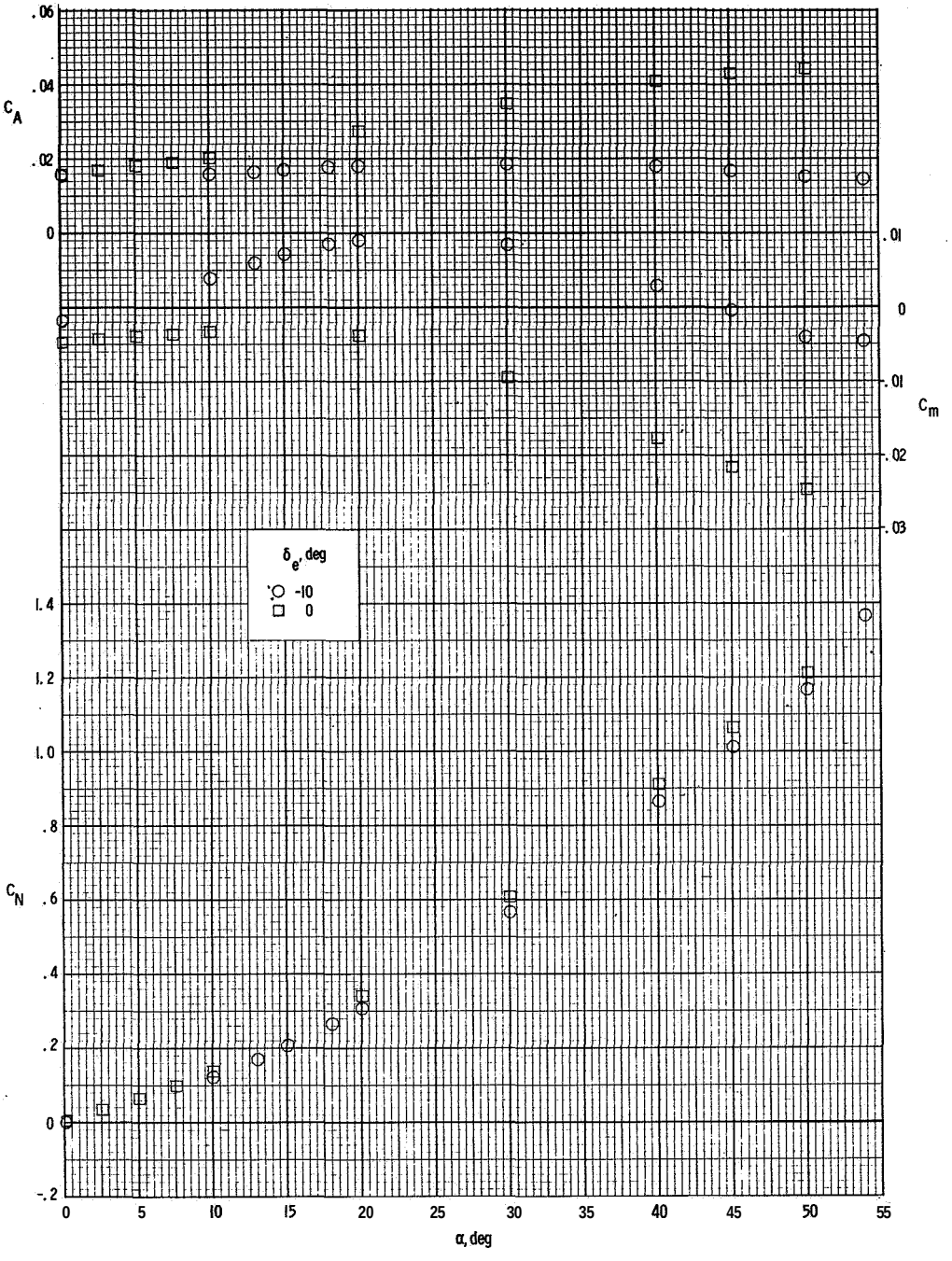

Figure 11.- Effect of elevon deflections on the aerodynamic characteristics of the baseline configuration with tip fins removed at M = 6 and R = 4.8×10^6.

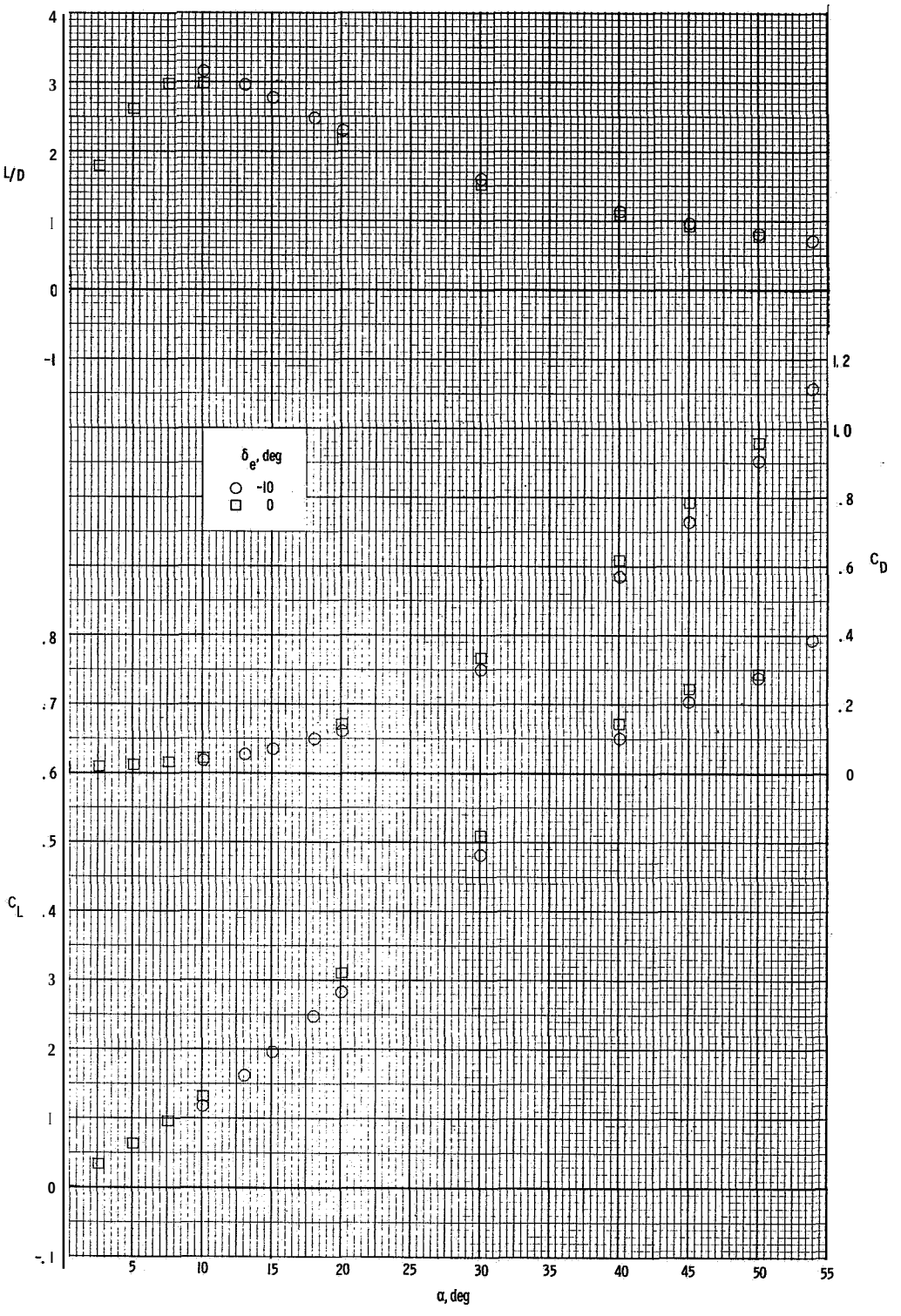

Figure 11.- Continued.

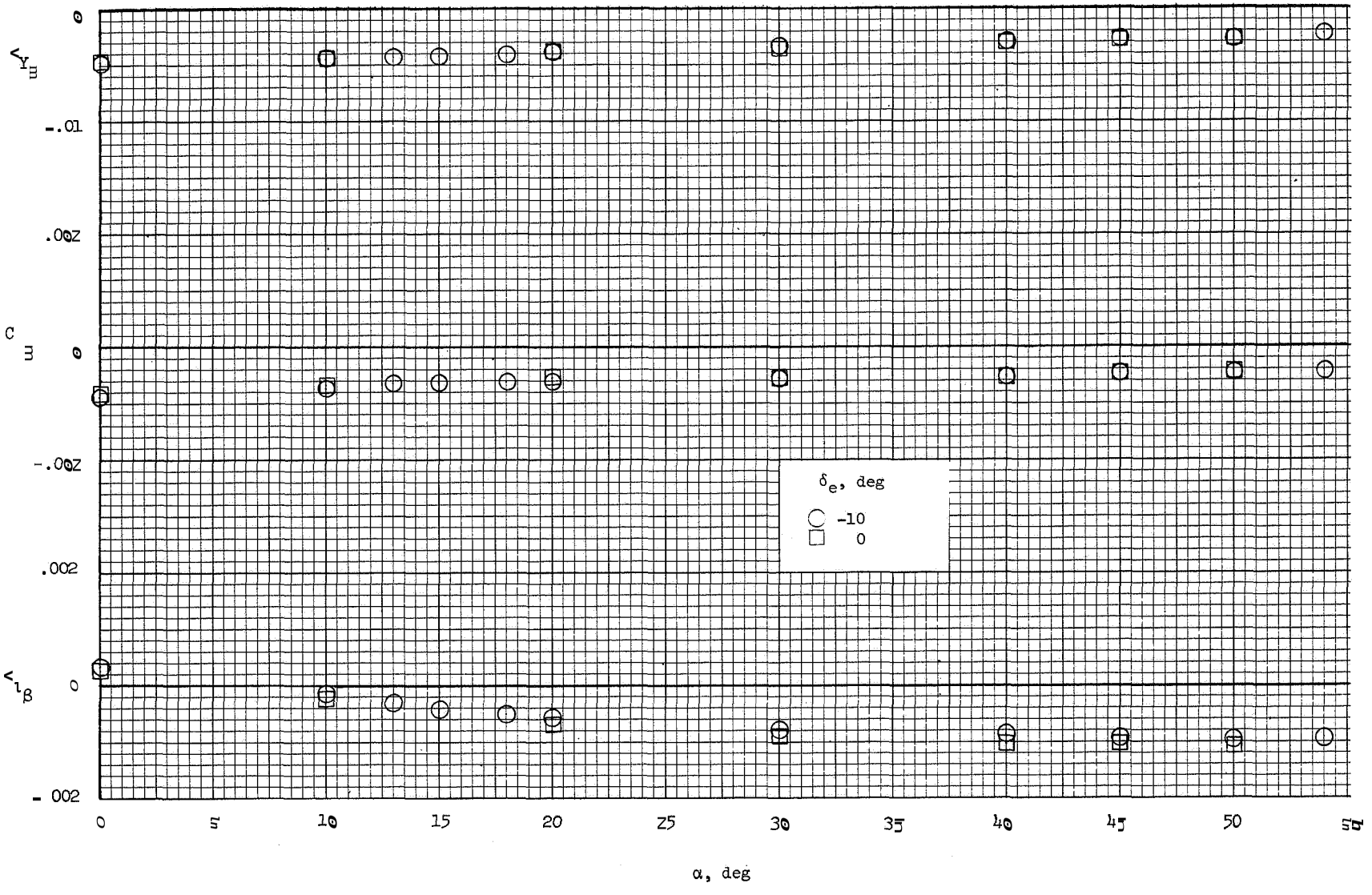

Figure 11.- Concluded.

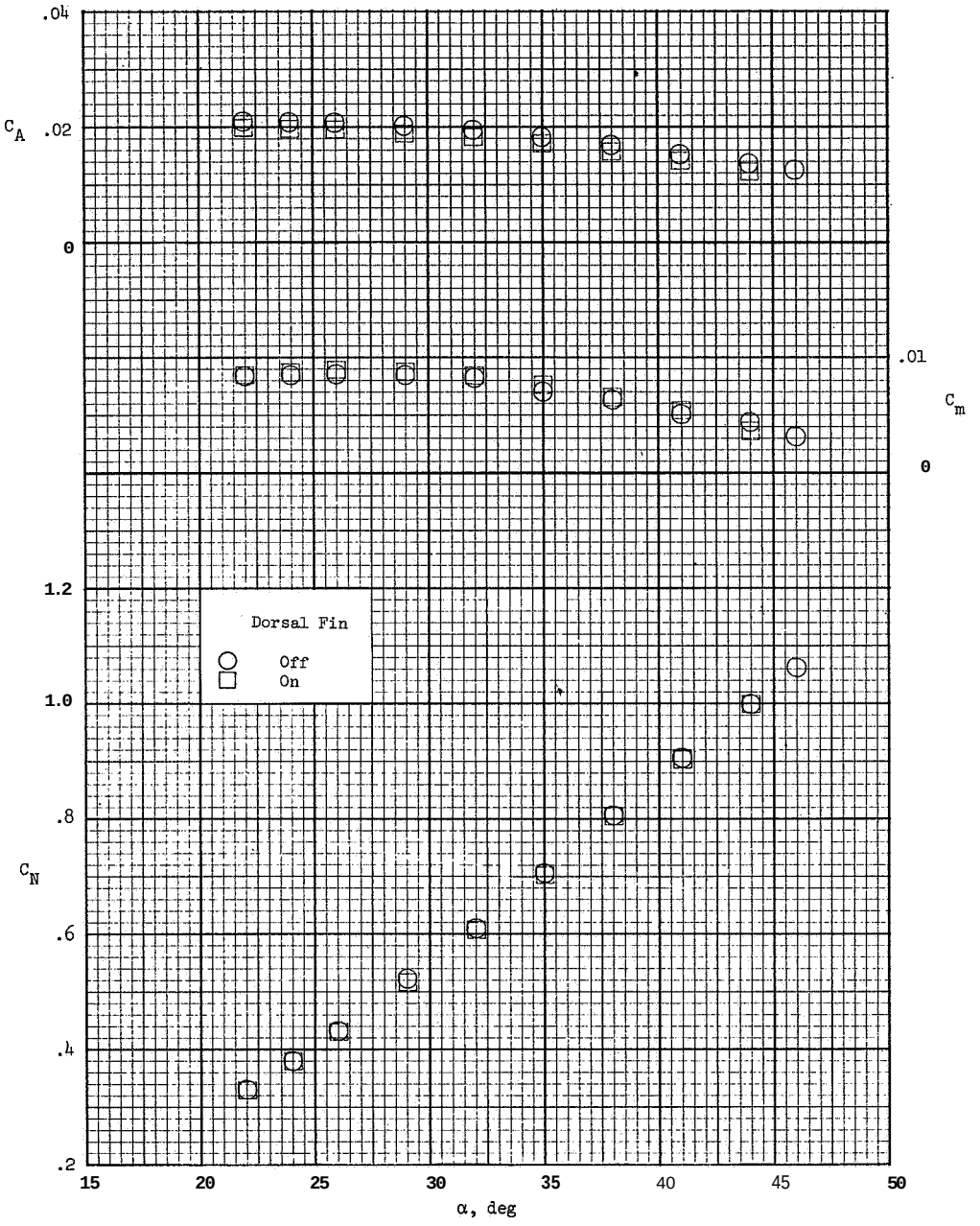

Figure 12.- Effect of the dorsal fin on the longitudinal aerodynamic characteristics for $\delta_e = -15^o$ on wing W_1 (no tip fins) at M = 20.6 and R = 2.9×10^6.

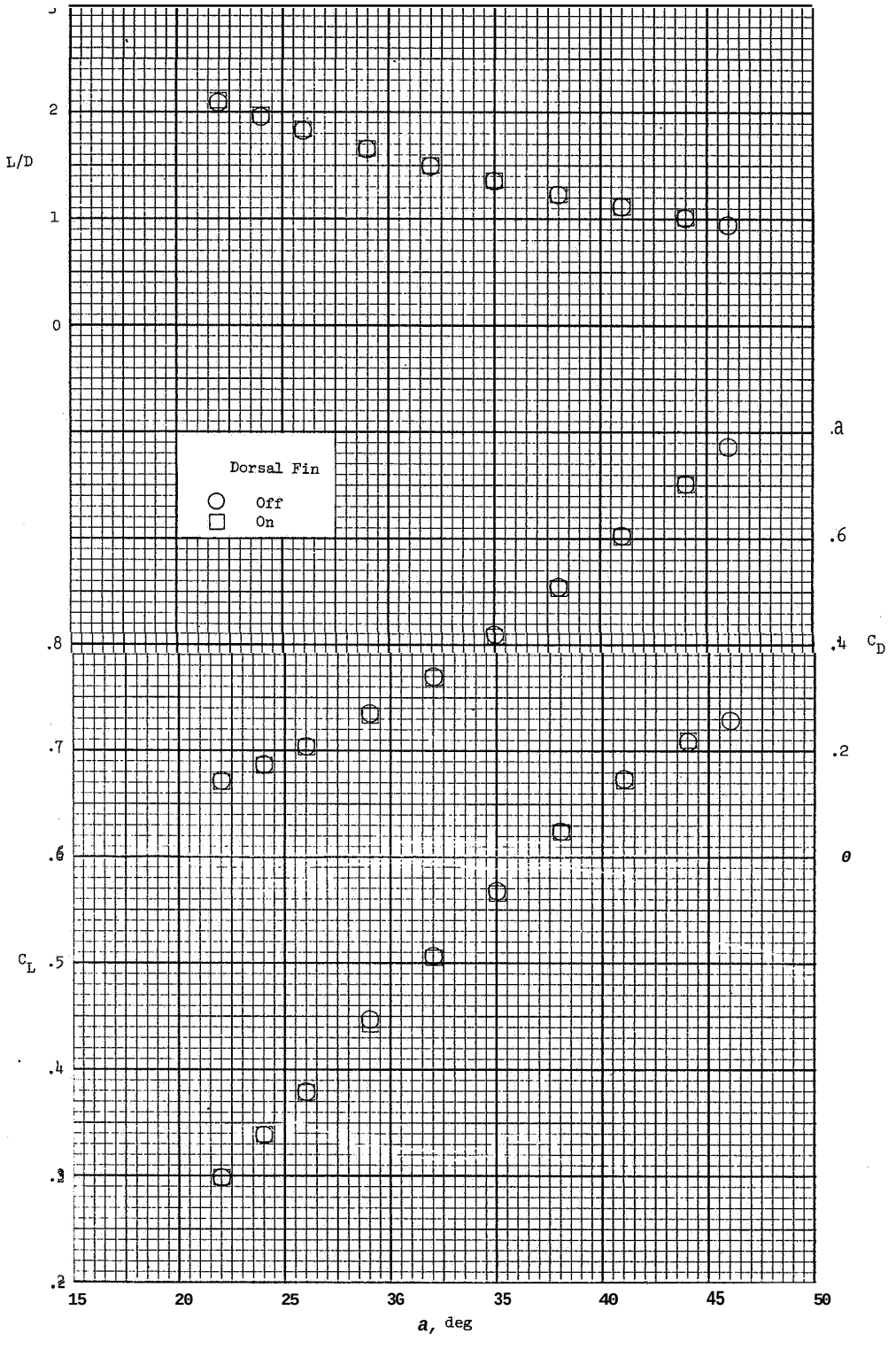

Figure 12.- Concluded.

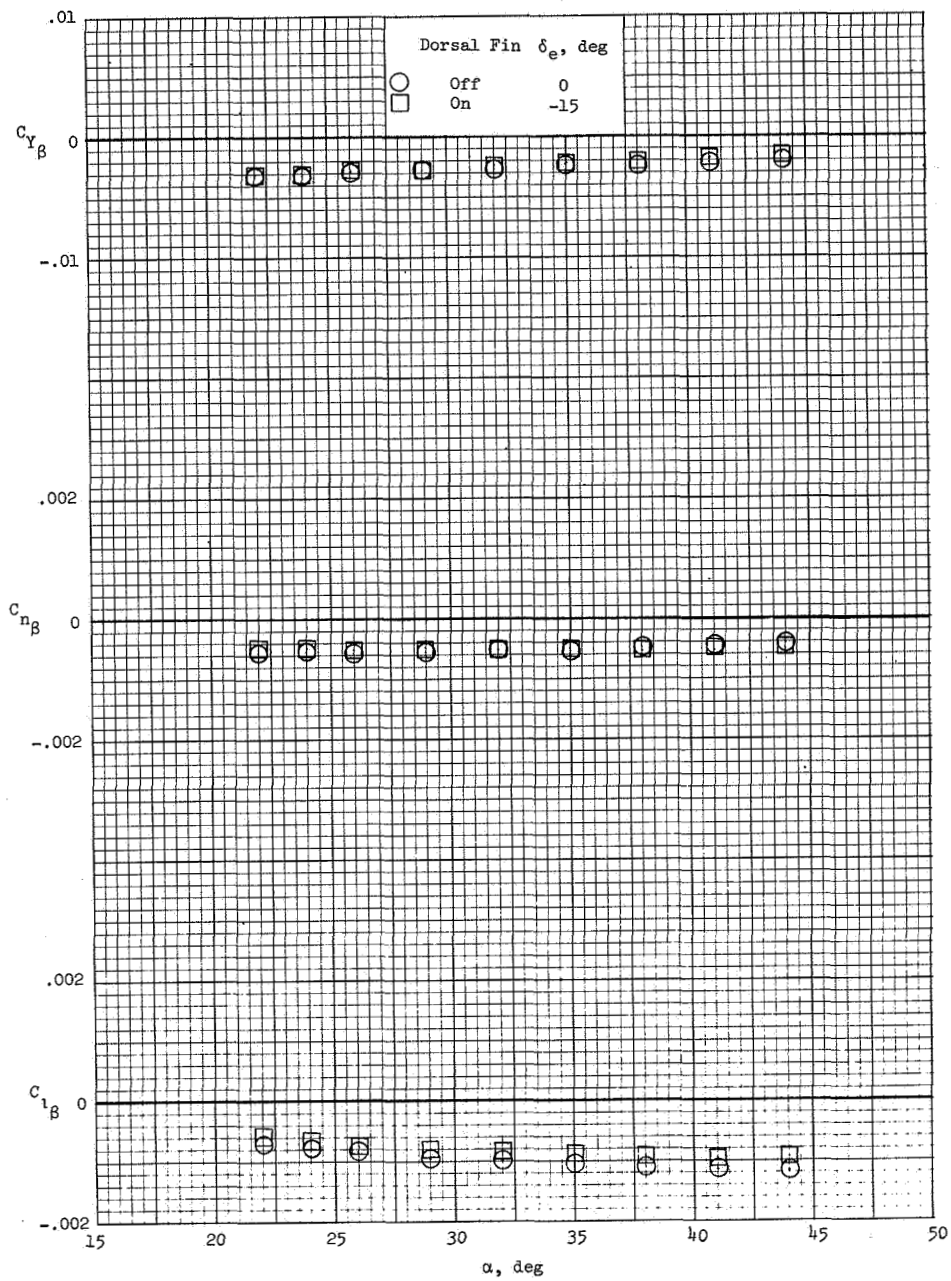

Figure 13.- Effect of the dorsal fin on the lateral and directional stability derivatives for two elevon deflections on wing W_1 at M = 20.6 and R = 2.9×10^6.

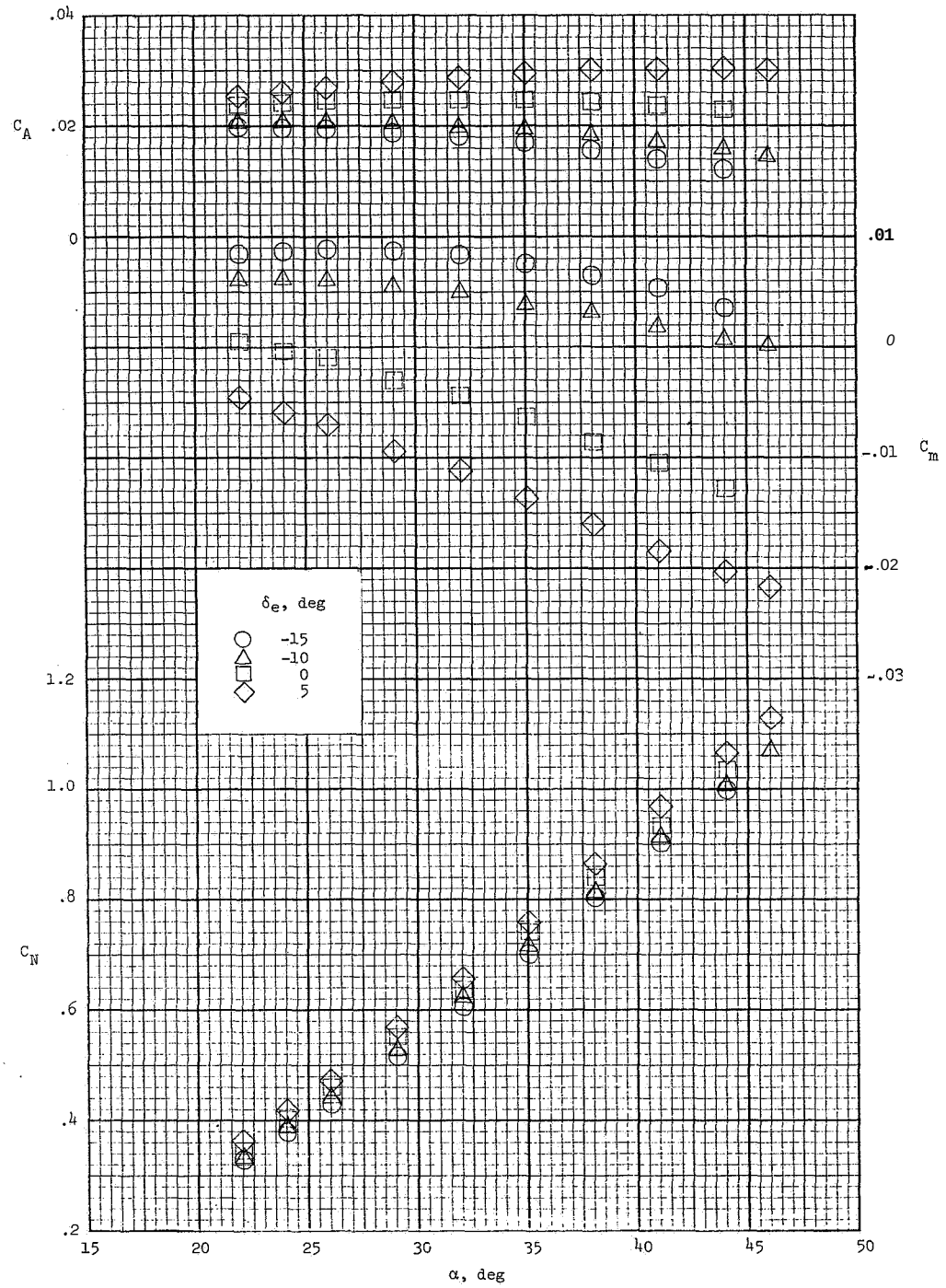

Figure 14.- Effect of elevon deflections on the longitudinal aerodynamic characteristics with tip fins off of wing W_1 and with dorsal fin on at $M = 20.6$ and $R = 2.9 \times 10^6$ for $\delta_b = -10^o$.

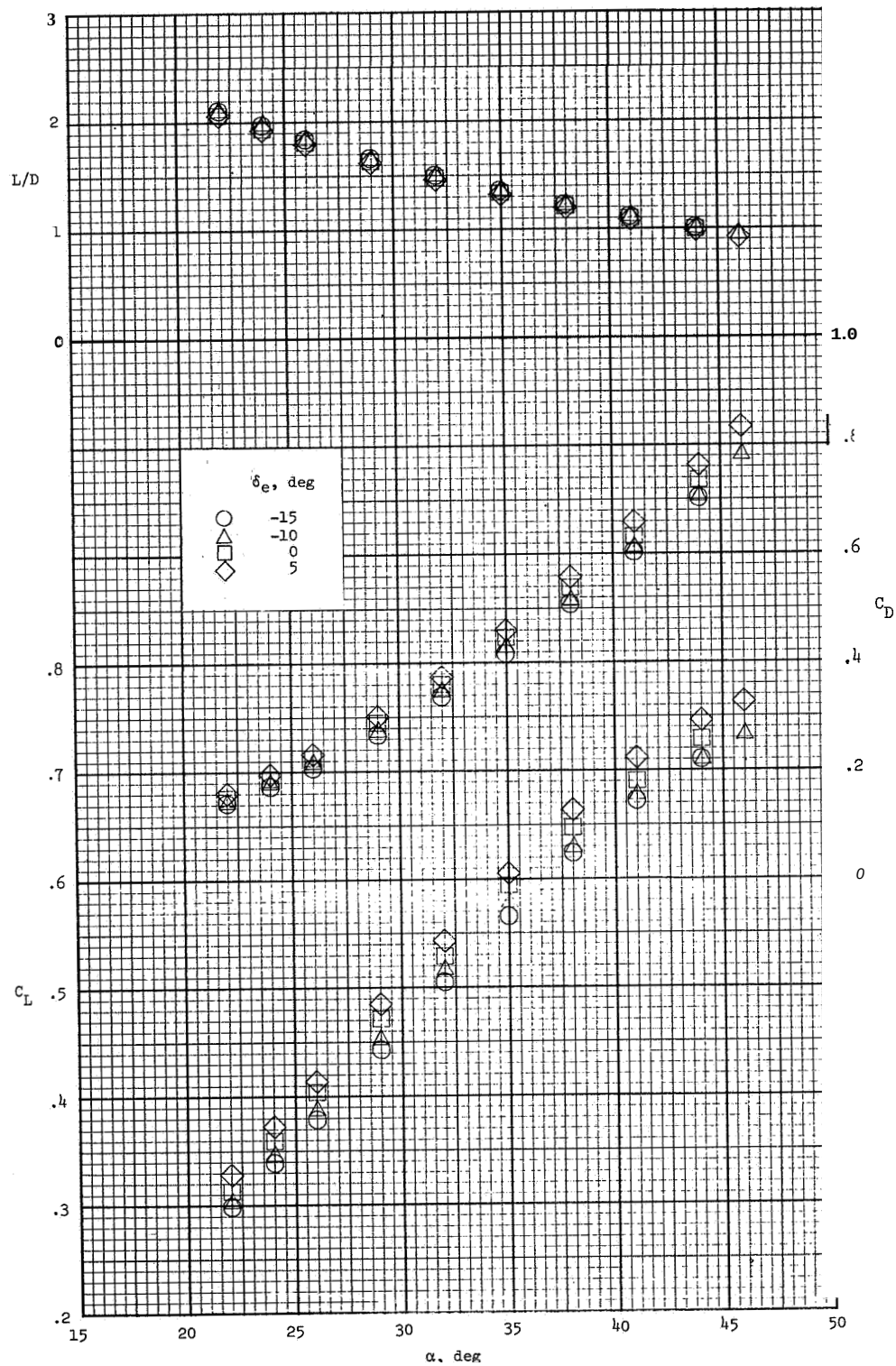

Figure 14.- Concluded.

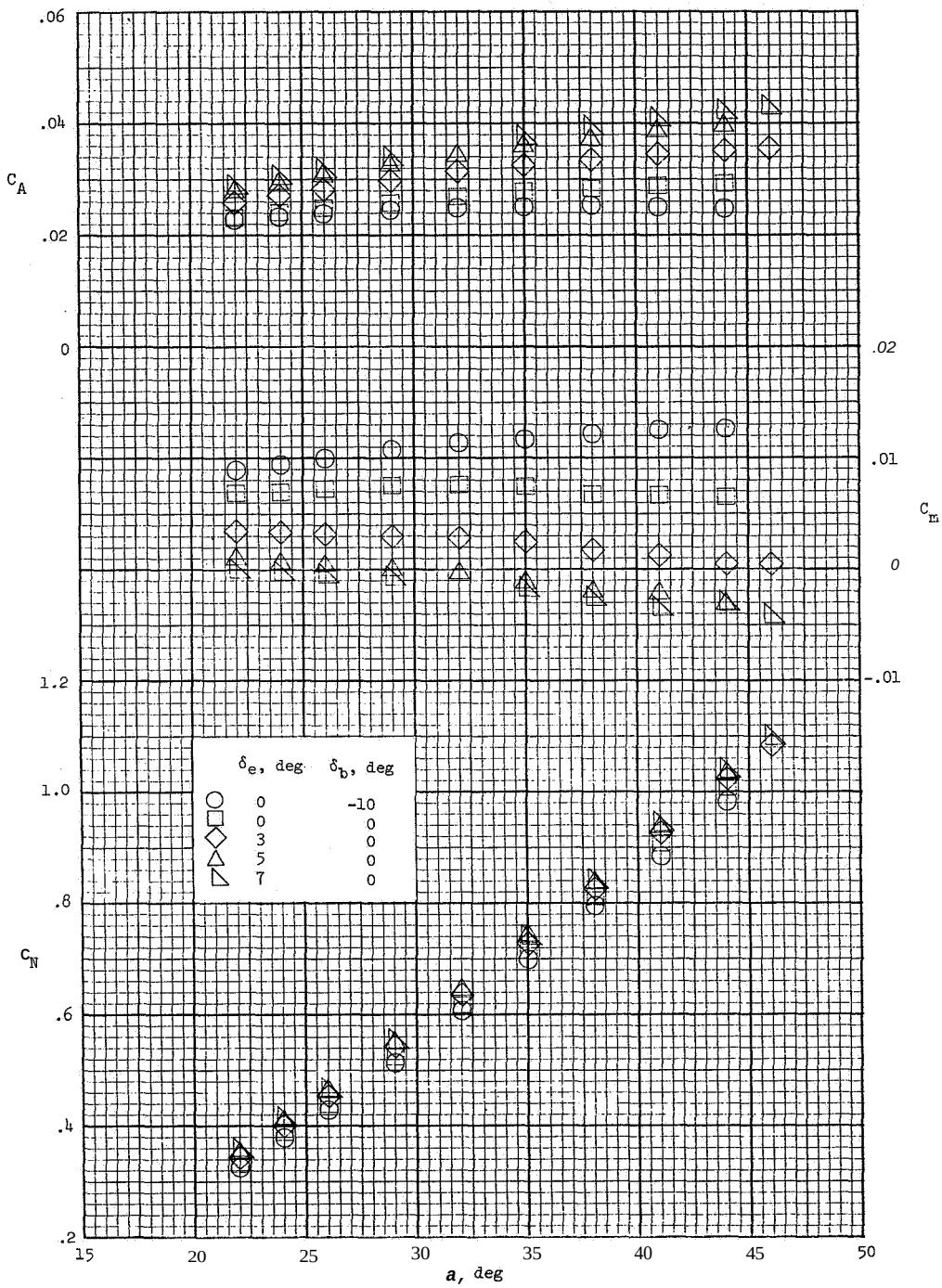

Figure 15.- Longitudinal aerodynamic characteristics using wing W_2 without a dorsal fin at M = 20.6 and R = 2.9 x 10^6.

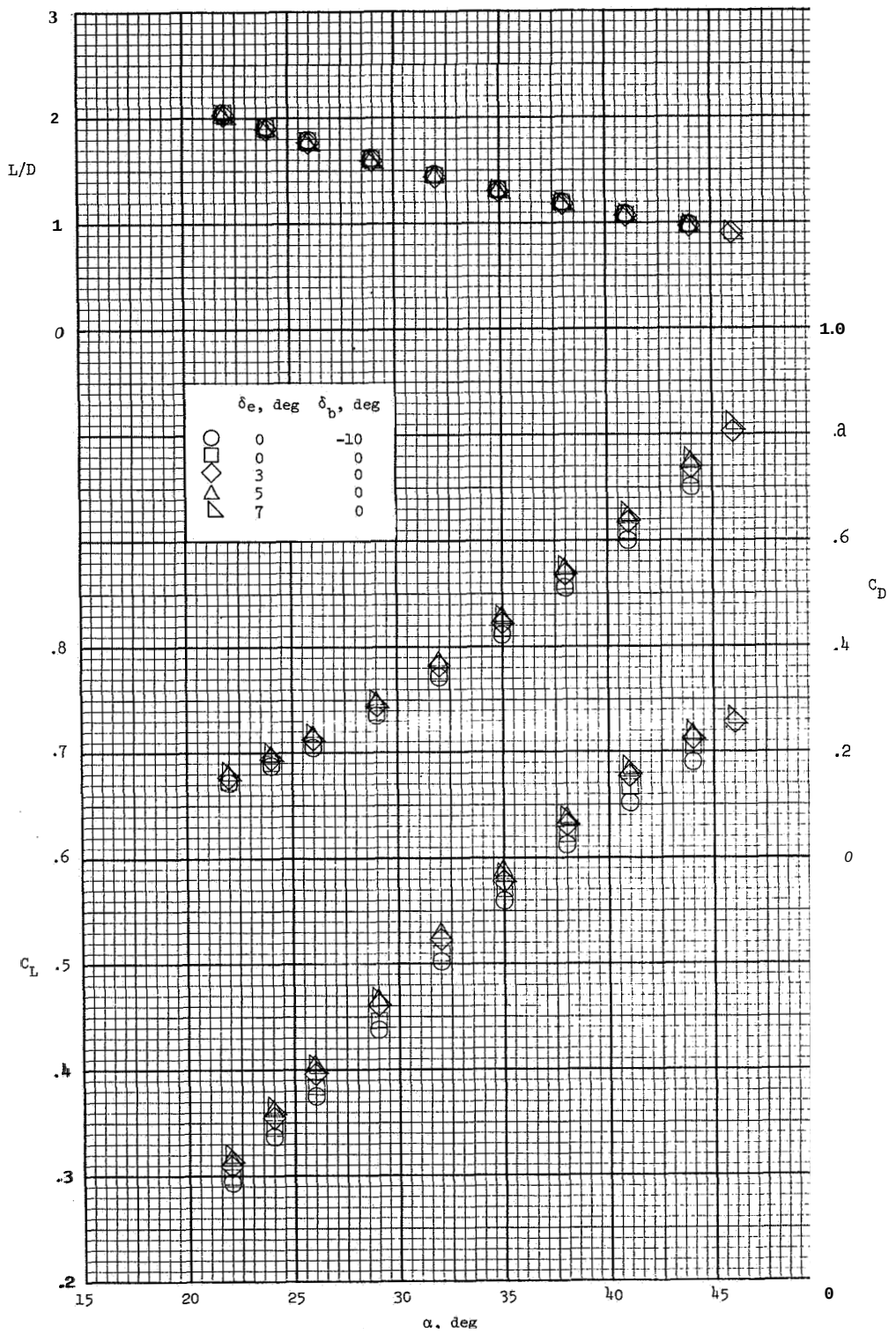

Figure 15.- Concluded.

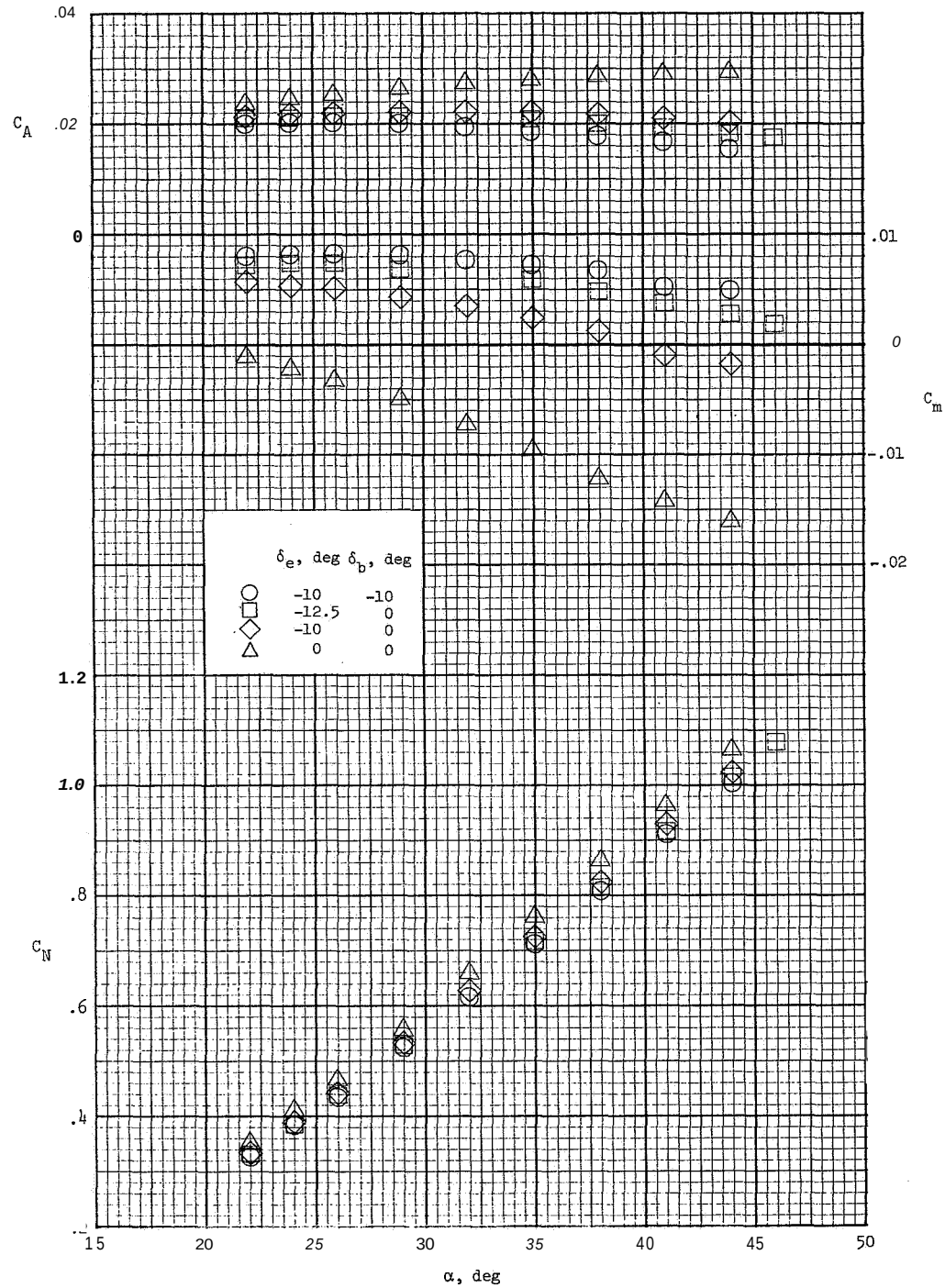

Figure 16.- Longitudinal aerodynamic characteristics using wing W_3 without a dorsal fin at M = 20.6 and $R = 2.9 \times 10^6$.

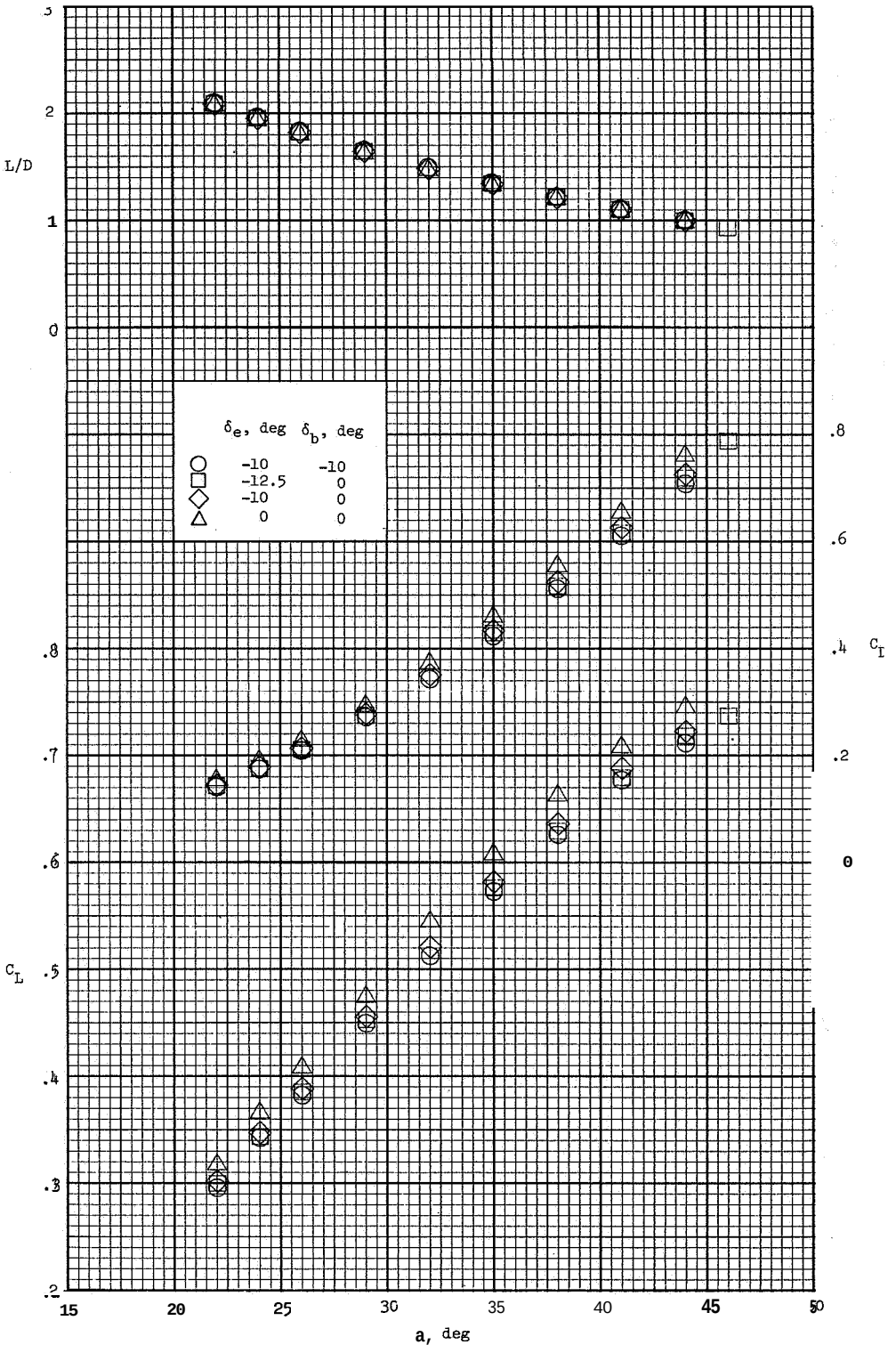

Figure 16.- Concluded.

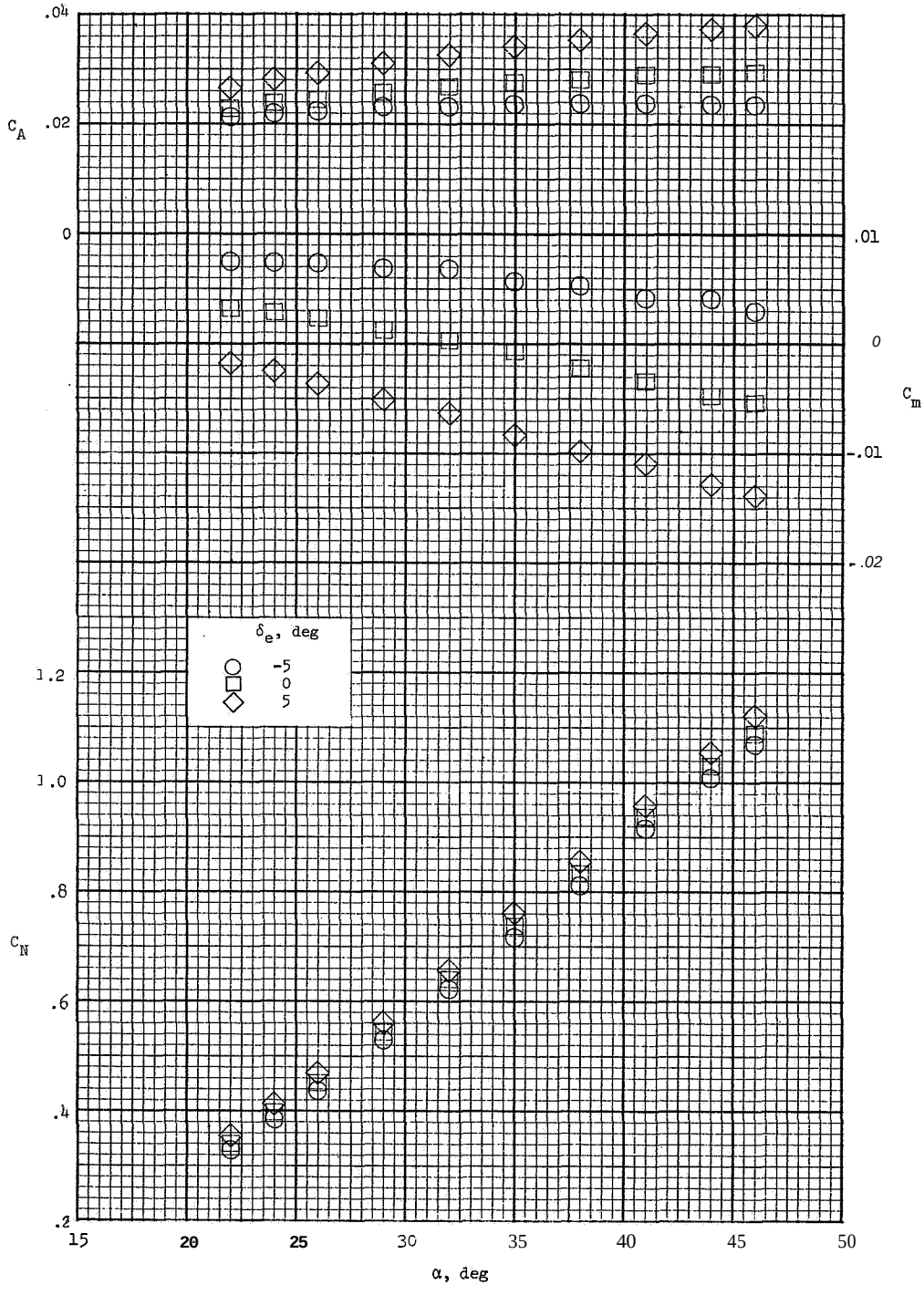

Figure 17.- Longitudinal aerodynamic characteristics using wing W_4 without a dorsal fin and with $\delta_b = 0^o$ at M = 20.6 and R = 2.9 x 10^6.

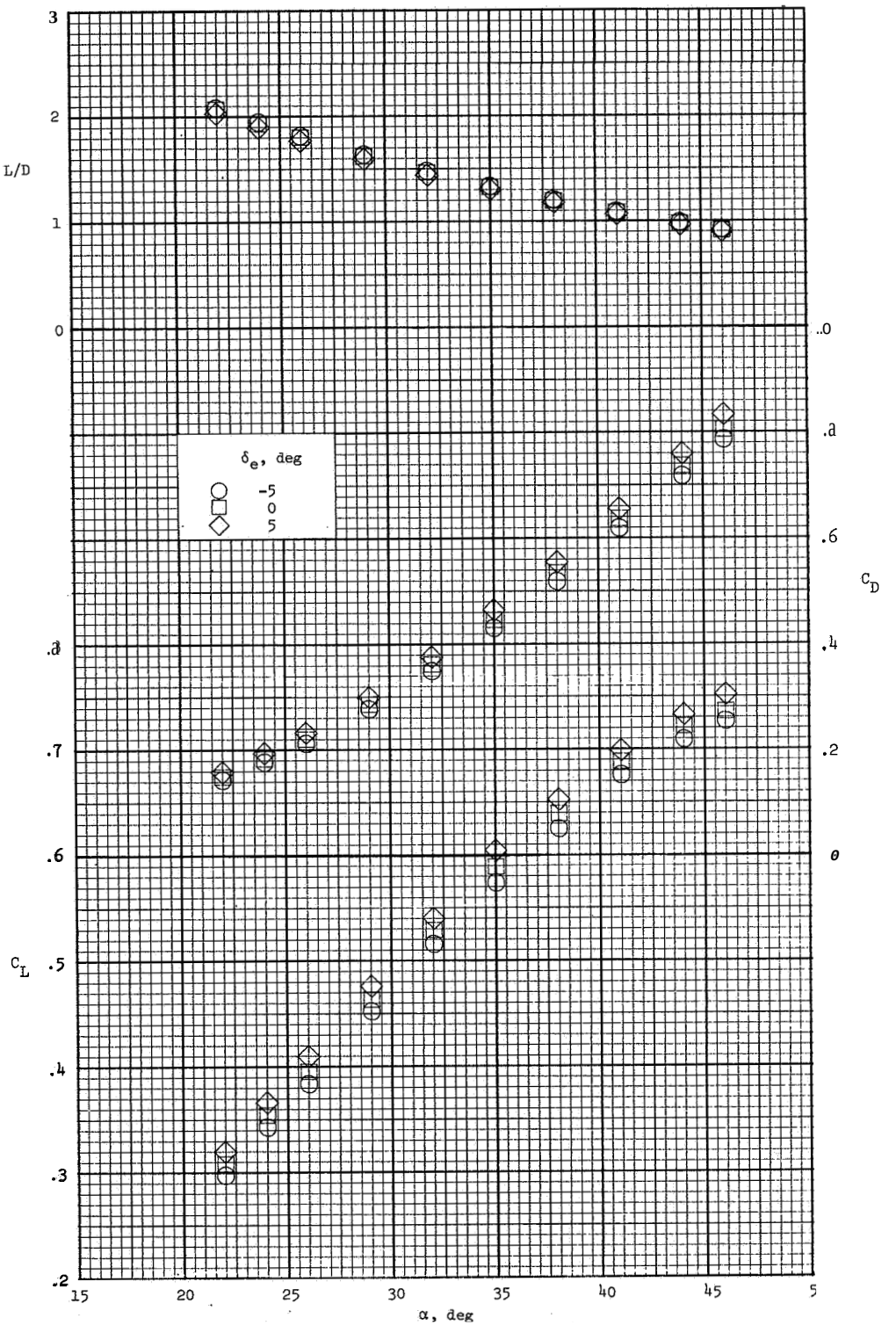

Figure 17.- Concluded.

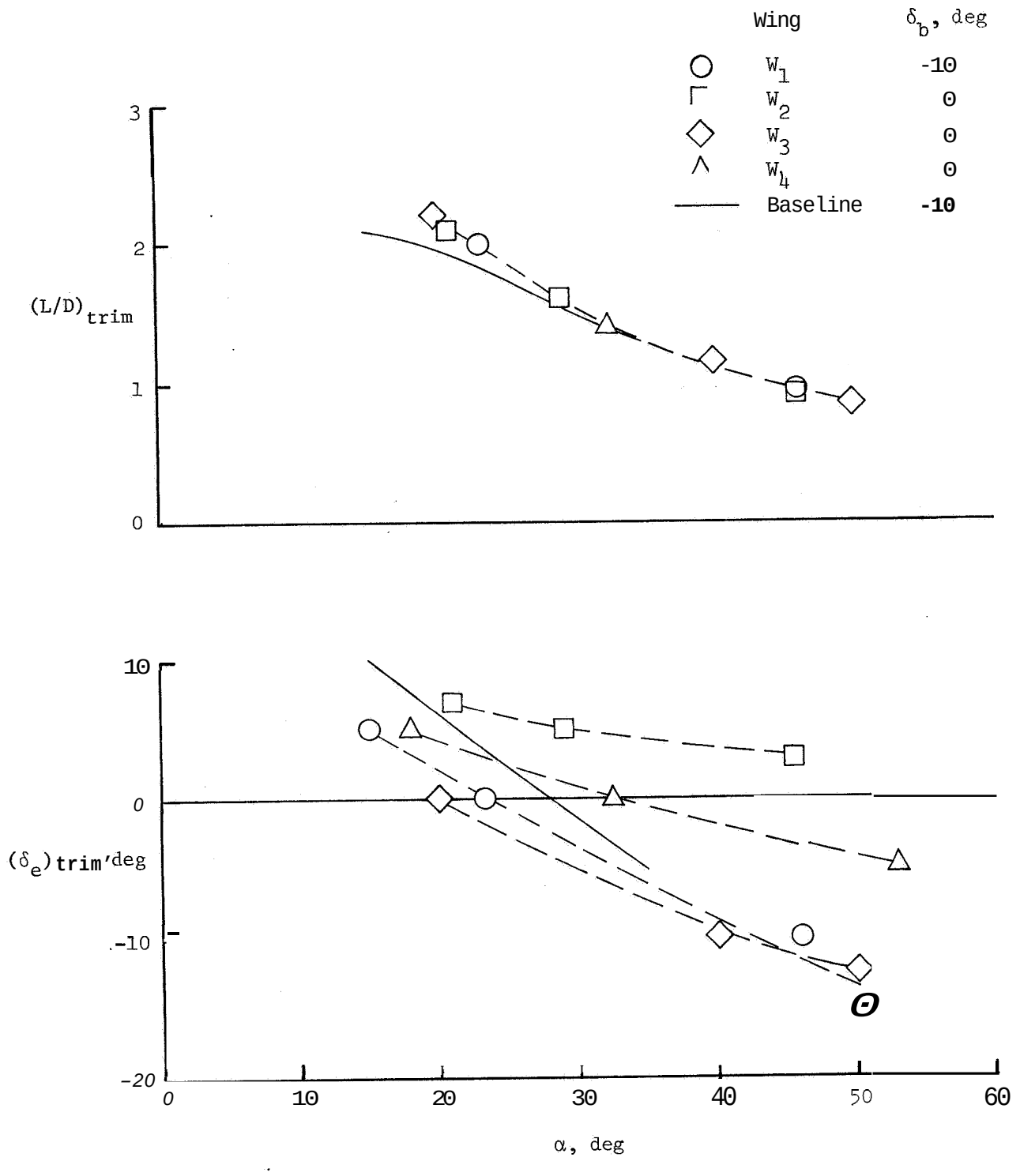

Figure 18.- Summary of wing-shape and elevon hinge-line sweep effects at M = 20.6 and R = 2.9×10^6.

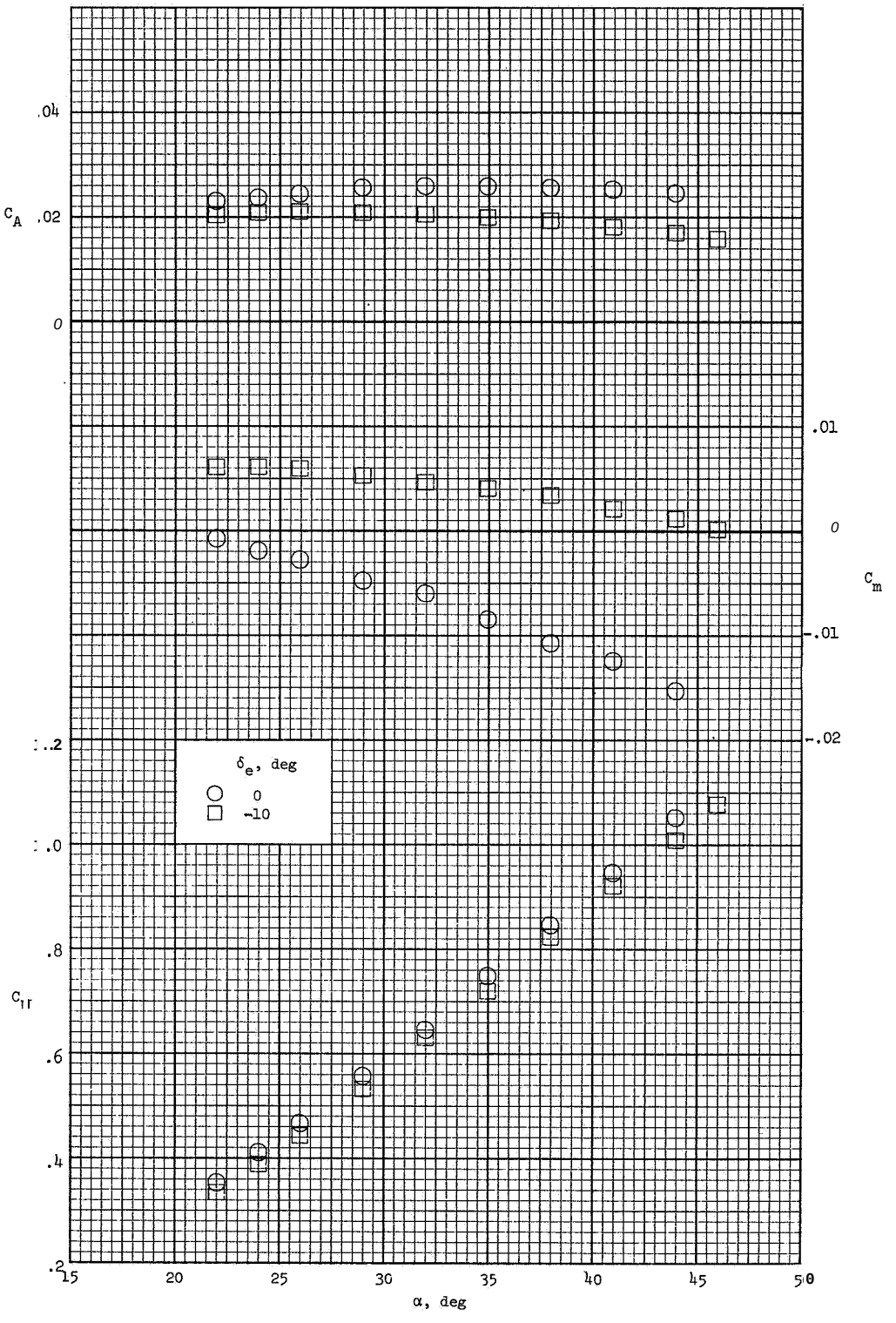

Figure 19.- Effect of elevon deflection on the longitudinal aerodynamic characteristics for $\delta_a = 5^o$ using wing W_1 with $\delta_b = -10^o$ at $M = 20.6$ and $R = 2.9 \times 10^6$.

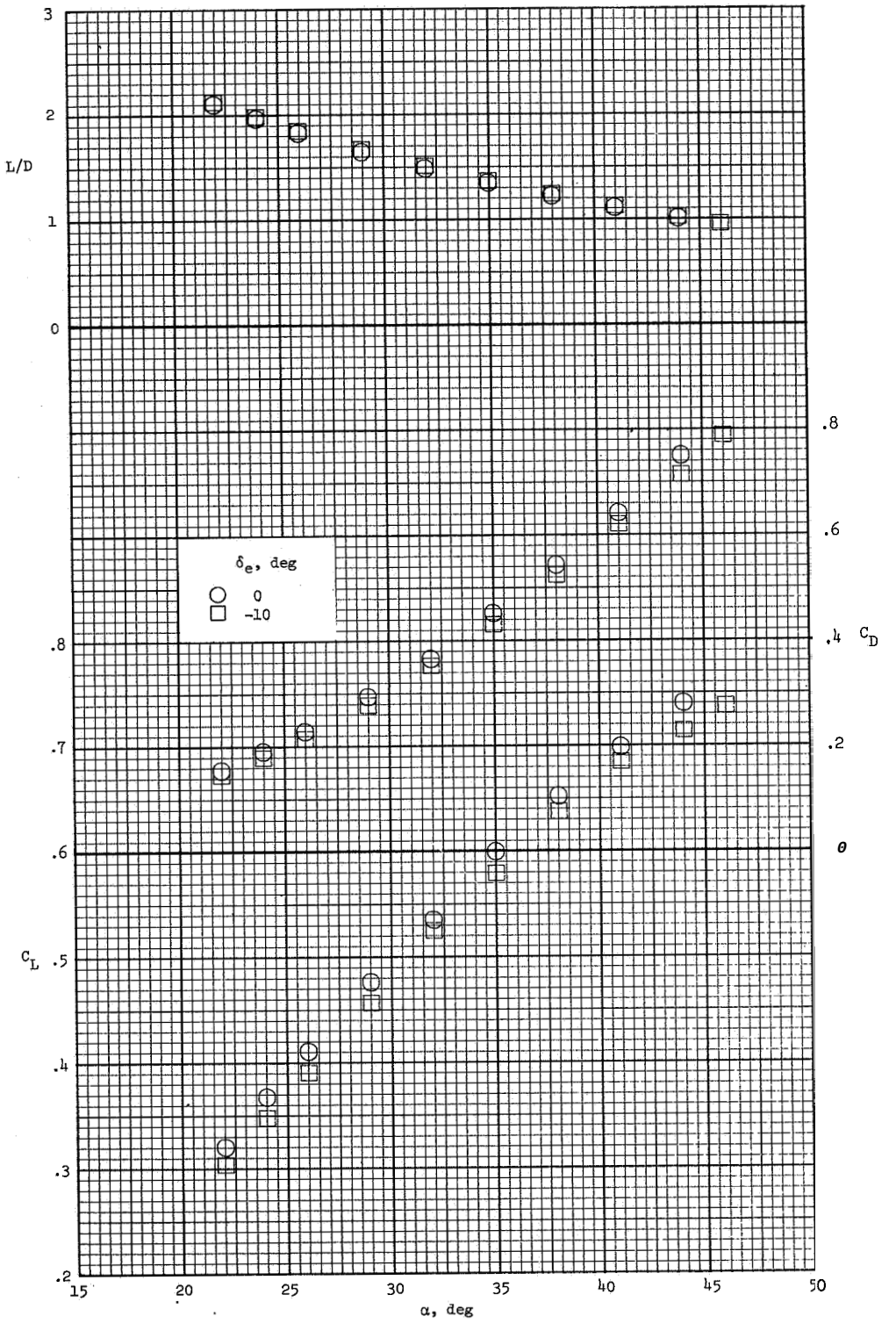

Figure 19.- Concluded.

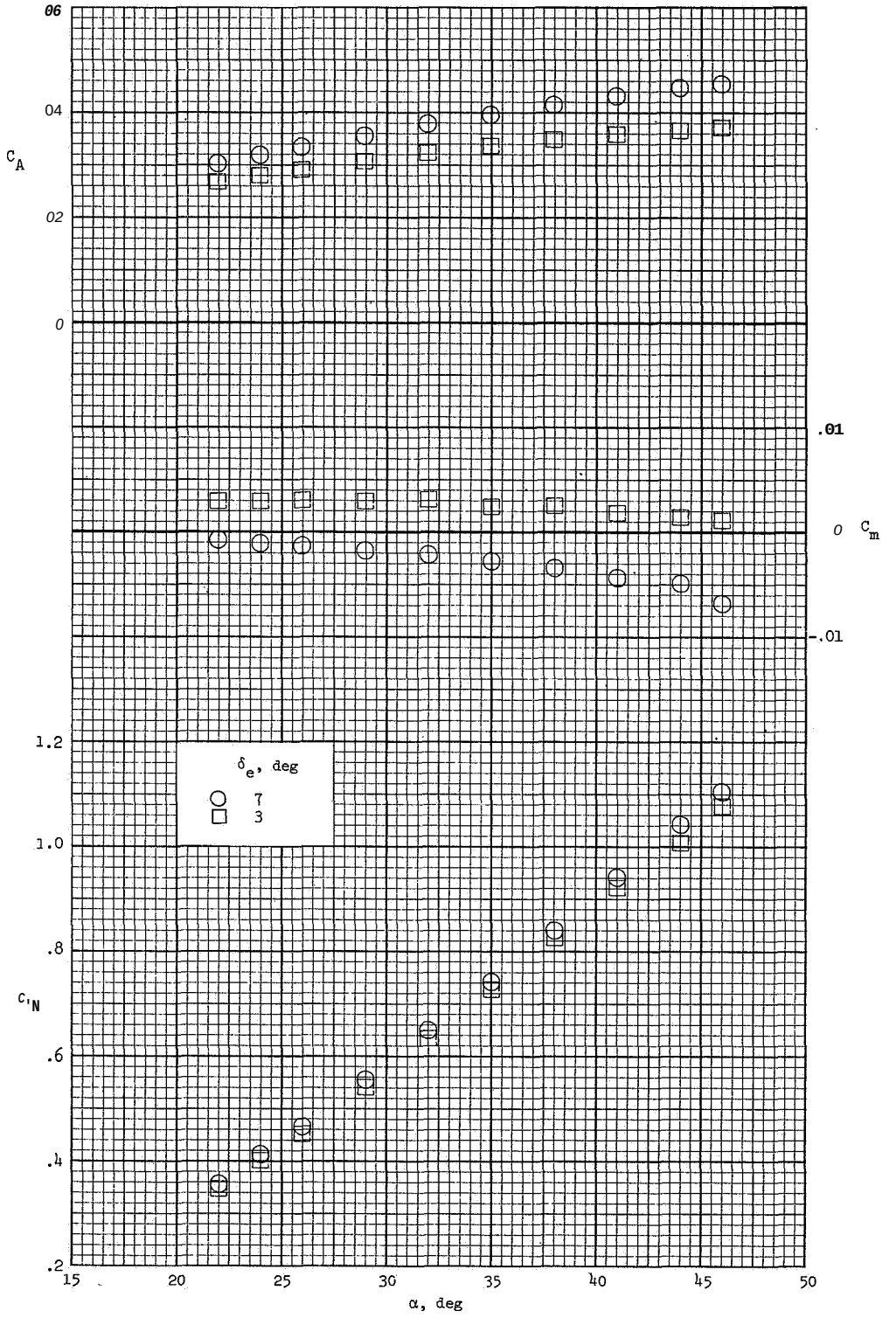

Figure 20.- Effect of elevon deflection on the longitudinal aerodynamic characteristics for $\delta_a = 5^o$ using W_2 with $\delta_b = 0^o$ at $M = 20.6$ and $R = 2.9 \times 10^6$.

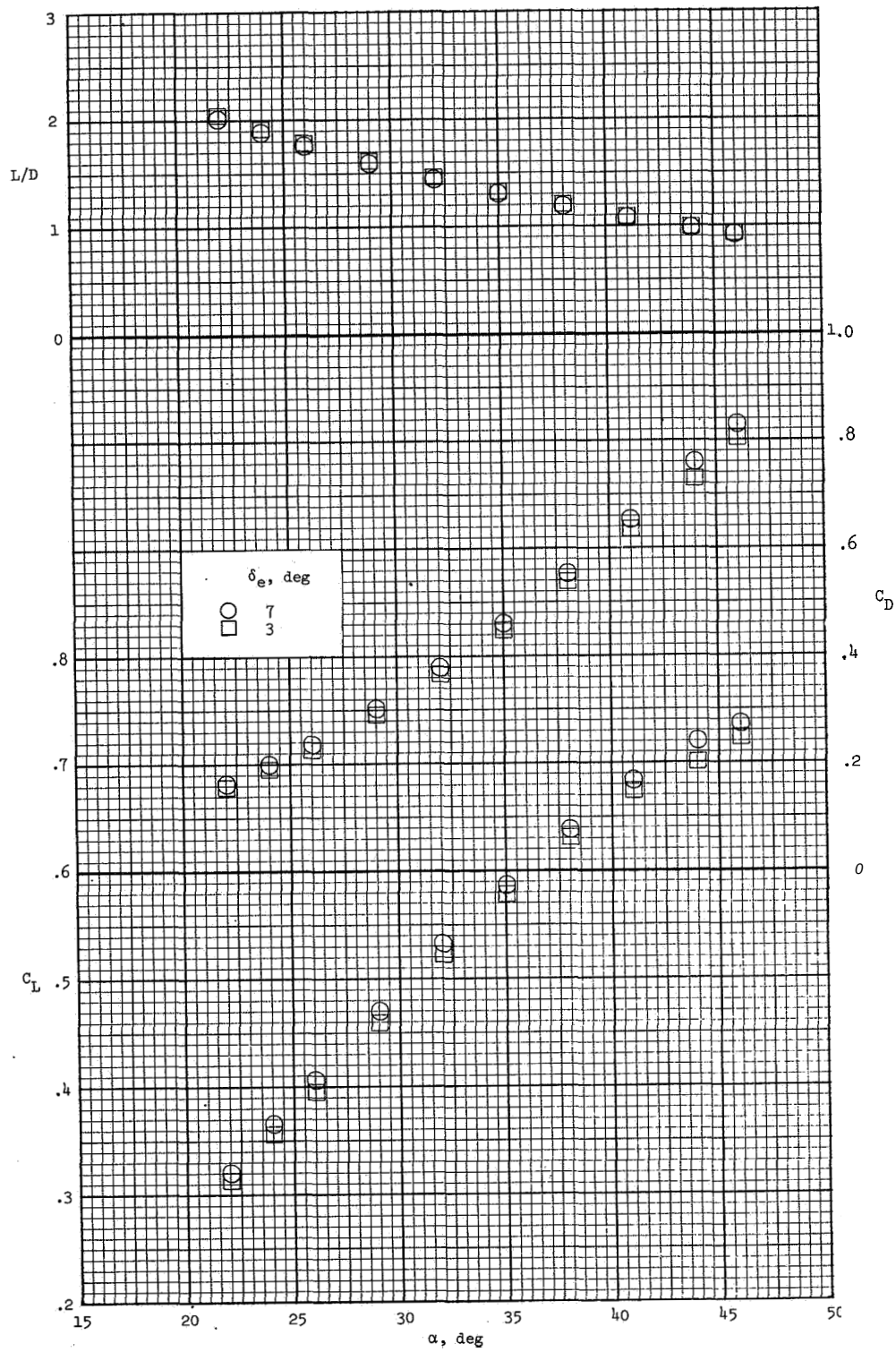

Figure 20. - Concluded.

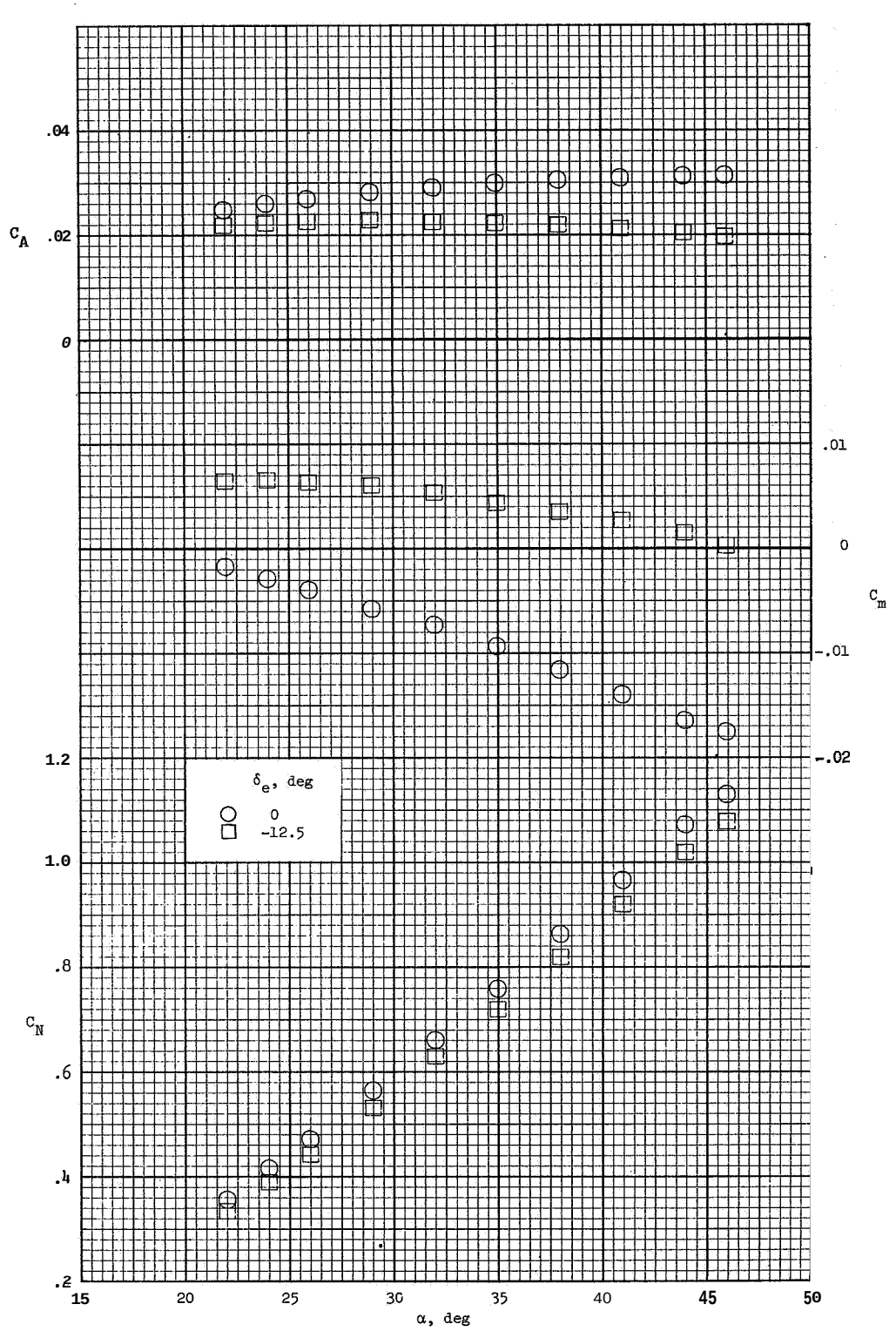

Figure 21. - Effect of elevon deflection on the longitudinal aerodynamic characteristics for $\delta_a = 5^o$ using wing W_3 with $\delta_b = 0^o$ at M = 20.6 and R = 2.9 x 10^6.

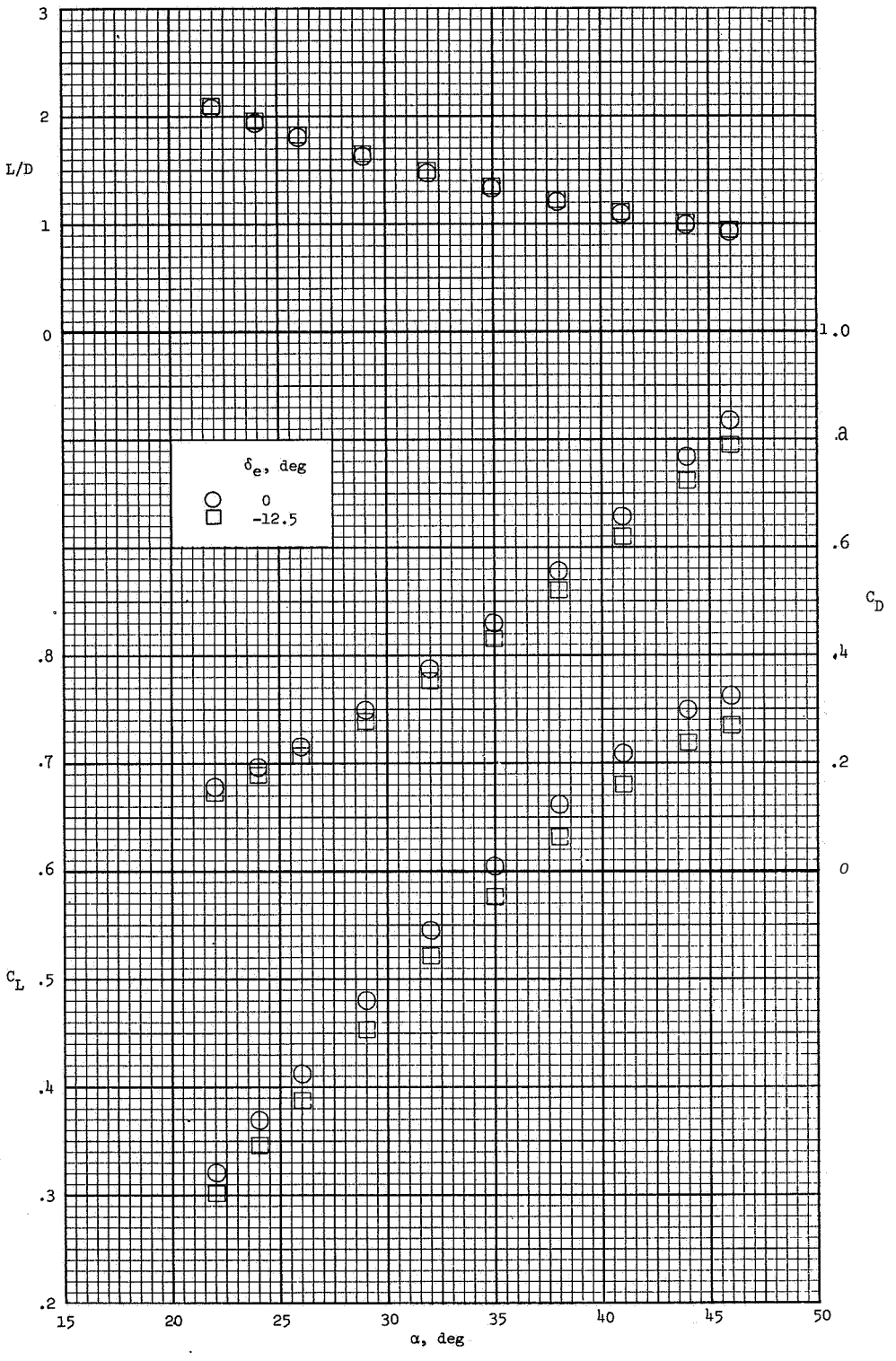

Figure 21.- Concluded.

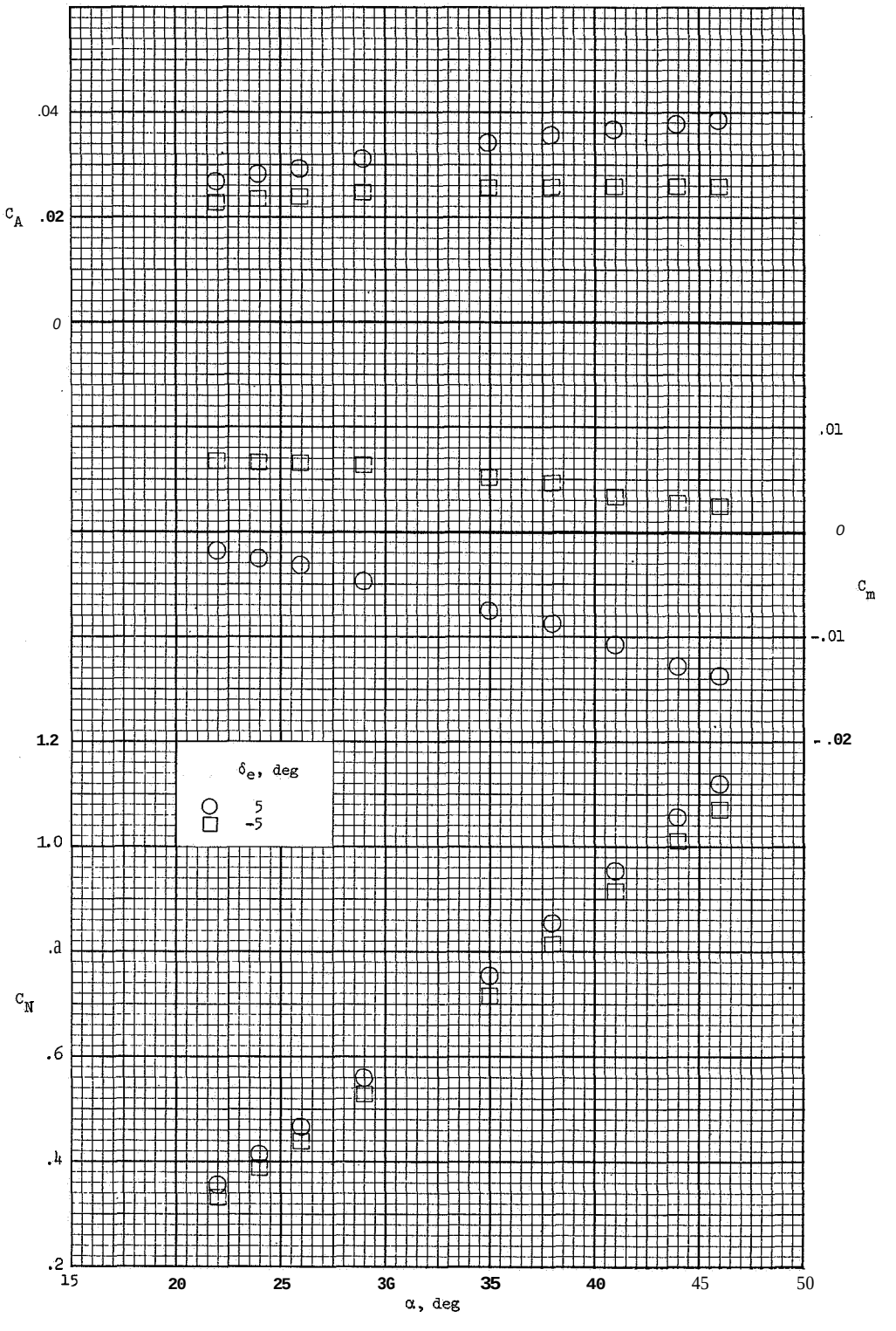

Figure 22.- Effect of elevon deflection on the longitudinal aerodynamic characteristics for $\delta_a = 5^o$ using wing W_4 with $\delta_b = 0^o$ at M = 20.6 and R = 2.9×10^6.

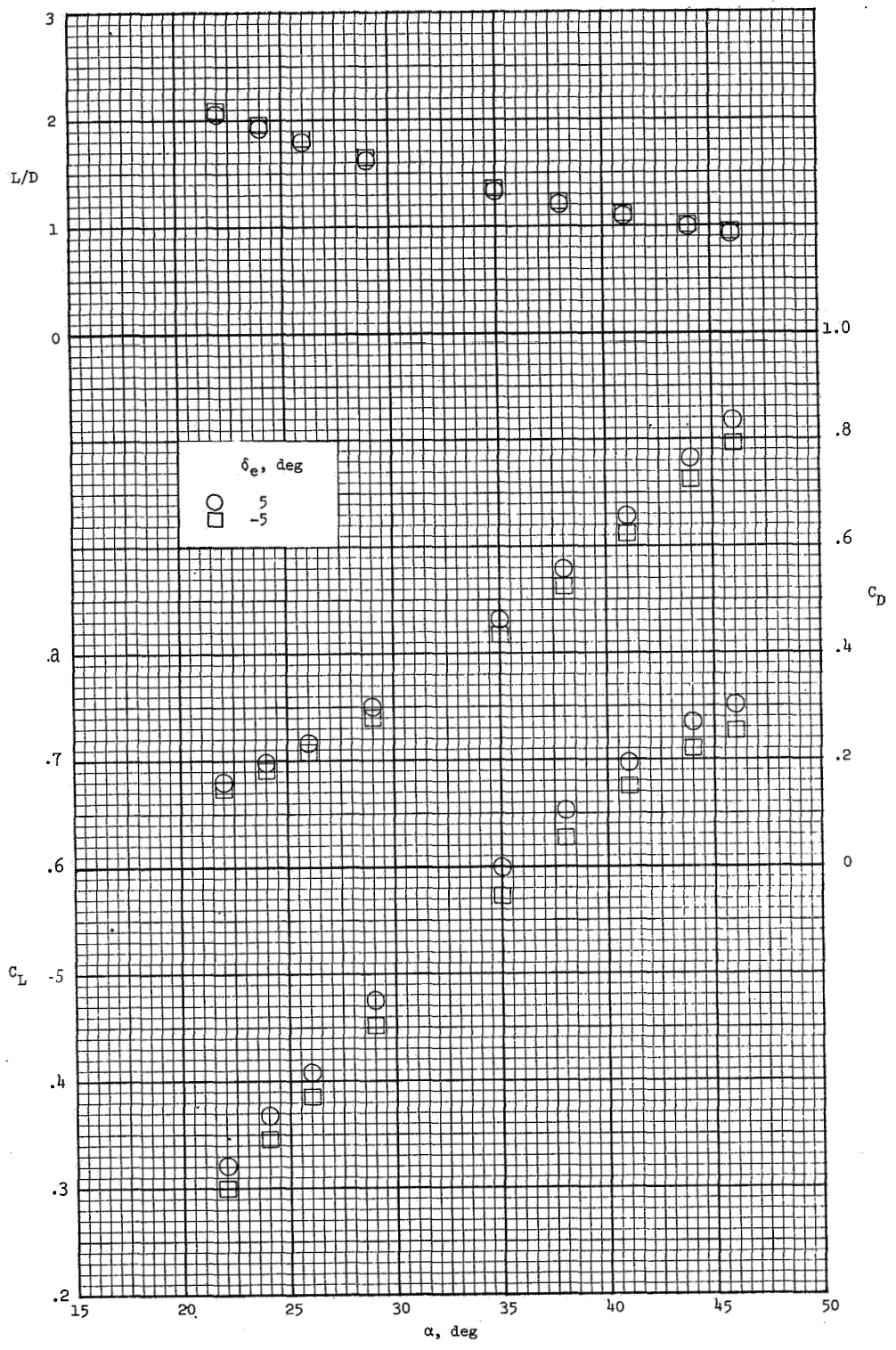

Figure 22. - Concluded.

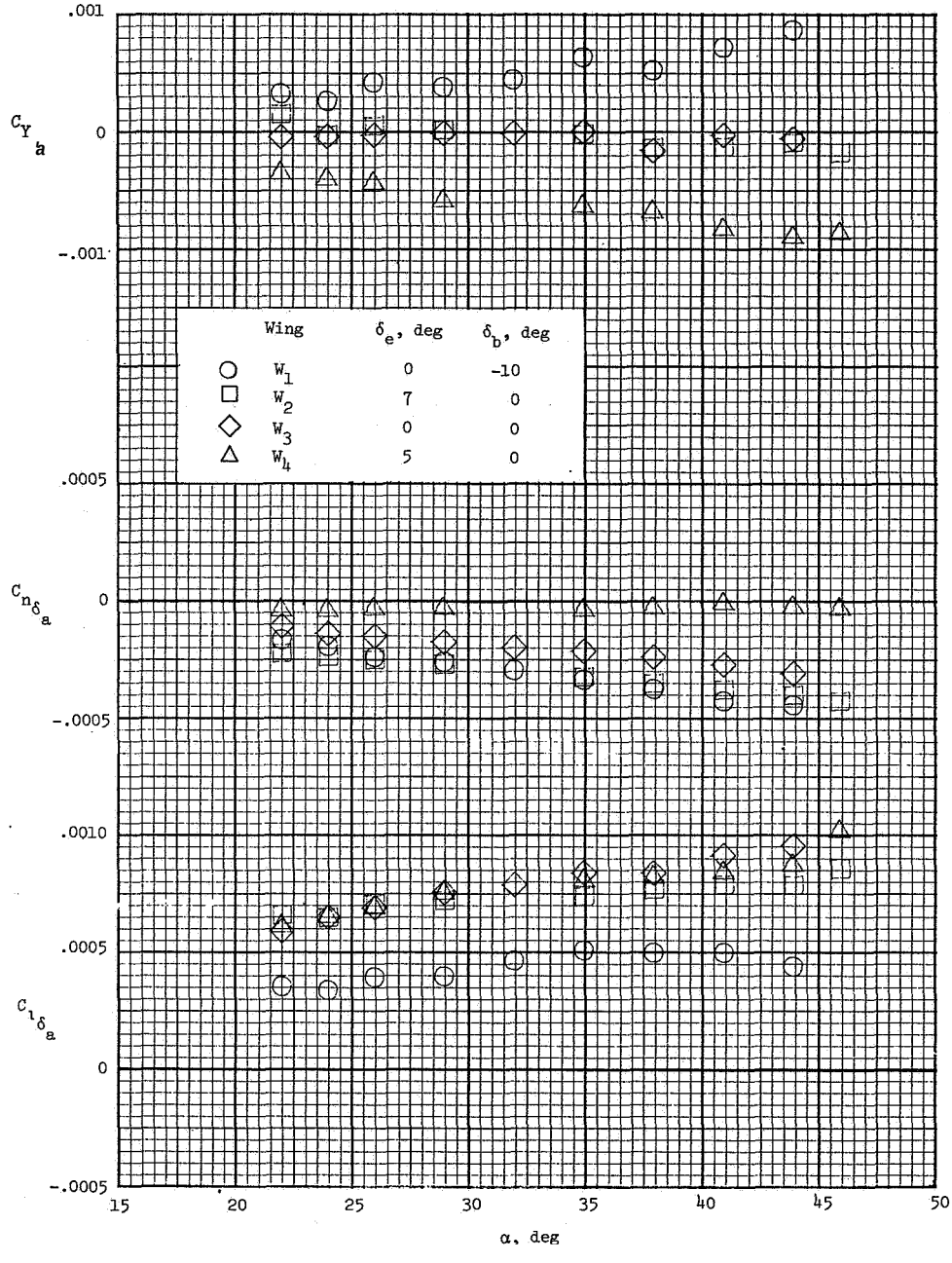

(a) LOW trim angles, $\alpha_{trim} \approx 20^{o}$.

Figure 23.- Lateral and directional control derivatives for the different wing shapes at M = 20.6 and R = 2.9 x 10^6.

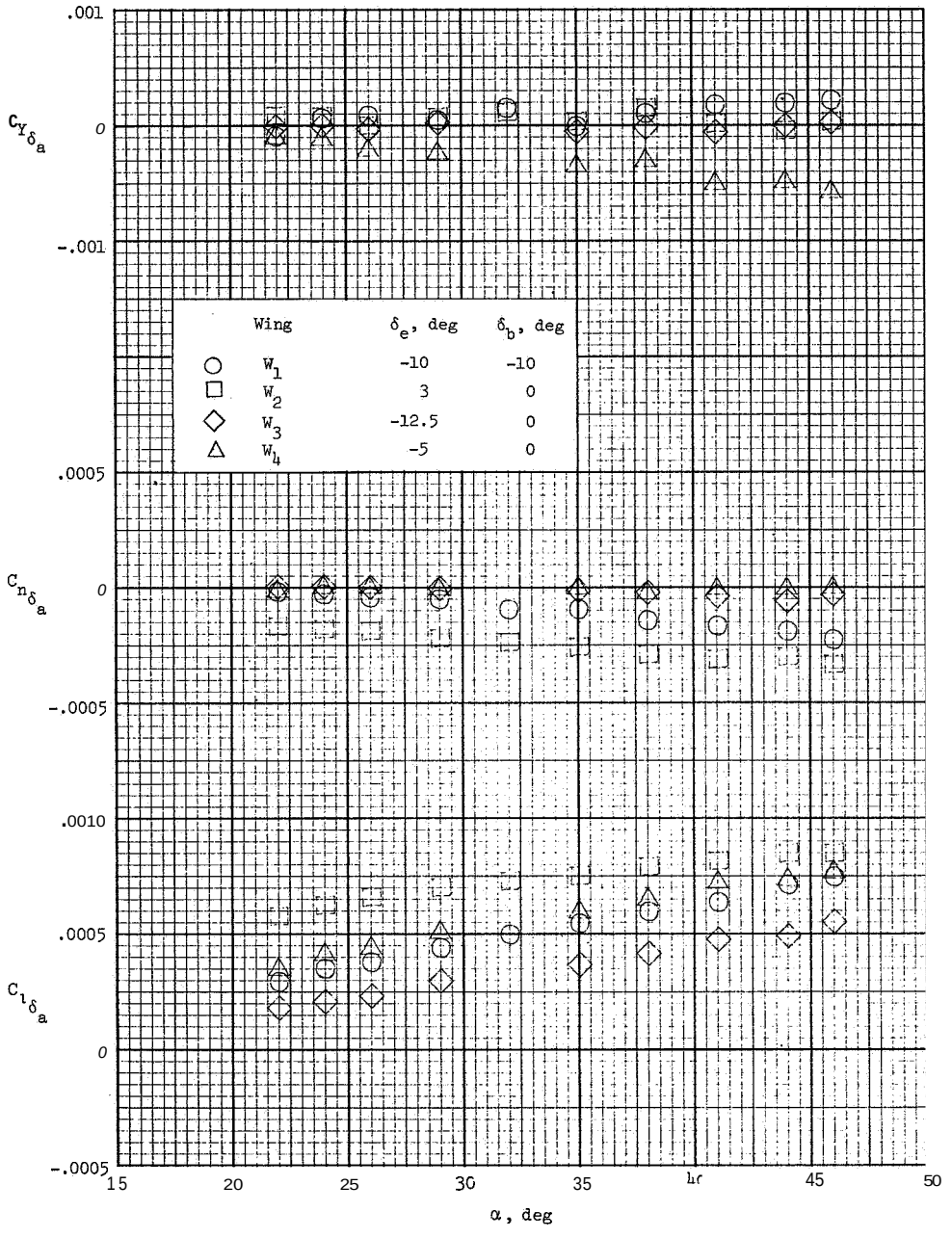

(b) High trim angles, $\alpha_{trim} \approx 47^{o}$.

Figure 23.- Concluded.